AD-A093 491 CNR INC NEEDHAM MA F/G 9/3
RADIO FREQUENCY MODELING OF AUDIO FREQUENCY SYSTEMS.(U)
OCT 80 J W GRAHAM, C J BOARDMAN, W WELCH F30602-78-C-0142
UNCLASSIFIED RADC-TR-80-331 NL

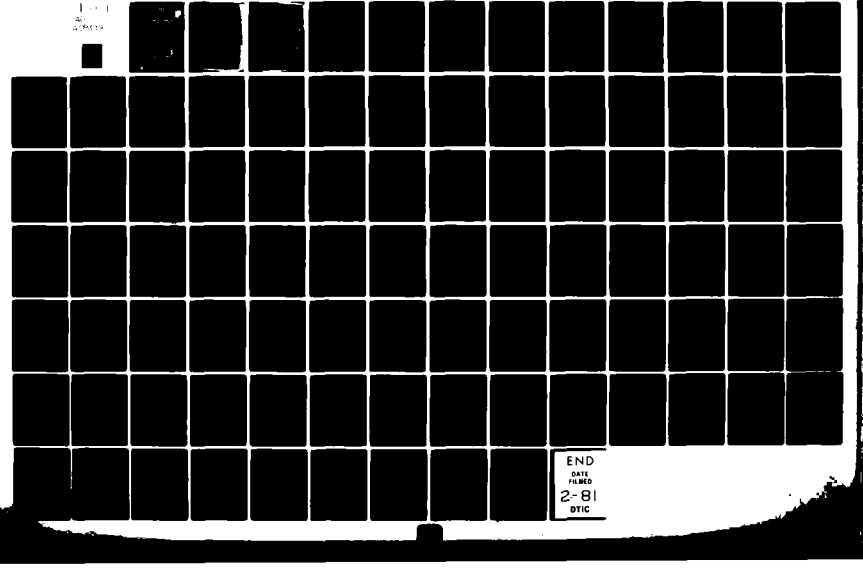

END
DATE FILMED
2-81
DTIC

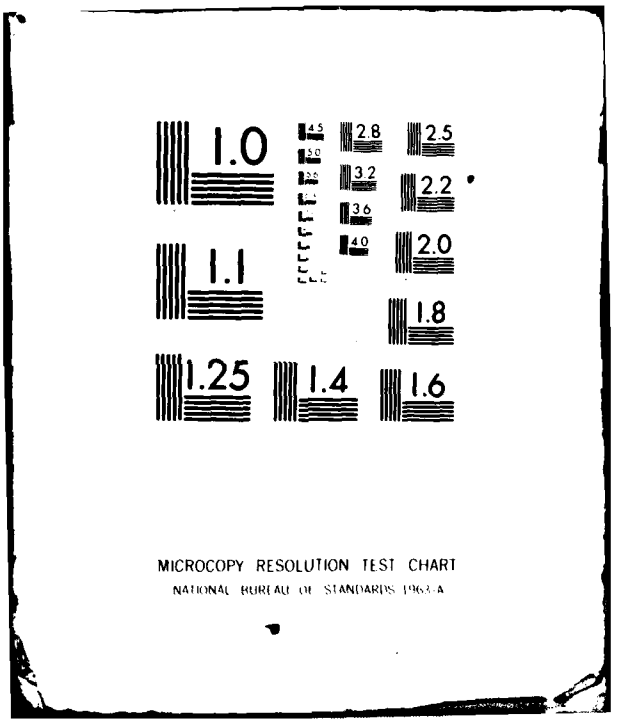
1.0
1.1
1.25
1.4
1.6
1.8
2.0
2.2
2.5
2.8
3.2
3.6
4.0
4.5
5.0
MICROCOPY RESOLUTION TEST CHART
NATIONAL BUREAU OF STANDARDS 1963-A

AD A093491

RADIO FREQUENCY AMPLIFIER AND AUDIO FREQUENCY SYSTEMS

CNR, Inc.

James W. Graham
Charles J. Reardon
William Welch

This report has been reviewed by the RADC Public [illegible]
in accordance to the National Technical Information [illegible]
it will be releasable to the general public, including [illegible]

RADC-TR-80-331 has been reviewed and is approved for [illegible]

APPROVED: Daniel E. Warren

DANIEL E. WARREN
Project Engineer

APPROVED: David C. Luke

DAVID C. LUKE, Colonel, USAF
Chief, Reliability & Compatibility Division

FOR THE COMMANDER: John P. [illegible]

JOHN P. [illegible]
Acting Chief, [illegible]

If your address has changed or if you wish to be removed from the
mailing list, or if the addressee is no longer employed by your
please notify RADC (RBCT) Griffiss AFB NY 13441. This will assist us in
maintaining a current mailing list.

Do not return this copy. Retain or destroy.

Rome Air

RADC plans and
selected
Communications
and engineering
is provided to
elements. The
communications,
veillance of
collection and
ionospheric
physics and
compatibility.

UNCLASSIFIED

SECURITY CLASSIFICATION OF THIS PAGE (When Data Entered)

REPORT DOCUMENTATION PAGE

READ INSTRUCTIONS BEFORE COMPLETING FORM

REPORT NUMBER: RADC-TR-80-331	2 GOVT ACCESSION NO: AD-A093 491
3 RECIPIENT'S CATALOG NUMBER	
TITLE (and Subtitle): RADIO FREQUENCY MODELING OF AUDIO FREQUENCY SYSTEMS	5 TYPE OF REPORT & PERIOD COVERED: Final Technical Report Sep 78 - Nov 79
	6 PERFORMING ORG. REPORT NUMBER: N/A
7 AUTHOR(s): James W. Graham, Charles J. Boardman, William Welch	8 CONTRACT OR GRANT NUMBER(s): F30602-78-C-0142
9 PERFORMING ORGANIZATION NAME AND ADDRESS: CNR, Inc. 220 Reservoir Street Needham MA 02194	10 PROGRAM ELEMENT, PROJECT, TASK AREA & WORK UNIT NUMBERS: 23380315
11 CONTROLLING OFFICE NAME AND ADDRESS: Rome Air Development Center (RBCT) Griffiss AFB NY 13441	12 REPORT DATE: October 1980
	13 NUMBER OF PAGES: 91
14 MONITORING AGENCY NAME & ADDRESS (if different from Controlling Office): Same	15 SECURITY CLASS. (of this report): UNCLASSIFIED
	15a DECLASSIFICATION DOWNGRADING SCHEDULE: N/A

16 DISTRIBUTION STATEMENT (of this Report)

Approved for public release; distribution unlimited.

17 DISTRIBUTION STATEMENT (of the abstract entered in Block 20, if different from Report)

Same

18 SUPPLEMENTARY NOTES

RADC Project Engineer: Daniel E. Warren (RBCT)

19 KEY WORDS (Continue on reverse side if necessary and identify by block number)

Nonlinear Distortion
Case Excitation
Nonlinear Circuit Analysis Distortion
Radio Frequency Modeling
Electromagnetic Compatibility
Nonlinear Circuit Models

20 ABSTRACT (Continue on reverse side if necessary and identify by block number)

The results of an effort to develop techniques for radio-frequency modeling at frequencies to 500 MHz of audio-frequency systems and their nonlinear response to amplitude-modulated excitation are reported. The approach involves investigation of a test amplifier to guide the modeling effort and to provide a means for validation measurements. The amplifier is conductively excited between its metal case and ground as well as at normal input terminals. Special techniques to avoid excitation of

(Cont'd)

DD FORM 1 JAN 73 1473 EDITION OF 1 NOV 65 IS OBSOLETE

UNCLASSIFIED

SECURITY CLASSIFICATION OF THIS PAGE (When Data Entered)

4 7 . 2

Item 20 (Cont'd)

indeterminate external modes were exployed. In addition to high-frequency models of electronic components with parasitic elements, it was necessary to develop wideband RF models for shielded ferrite-core low-frequency inductors. It was also necessary to include models of the printed-circuit etch. The physical geometry of component and printed-circuit layout played a significant role in the model development. The detection process for demodulation of amplitude-modulated radio carrier excitation was modeled in terms of the second-order nonlinear transfer functions. These functions were expressed in terms of the linear response of the wideband model at the nonlinearity and the low-freuqency response of the amplifier. Prediction of model linear and nonlinear responses over many decades of radio carrier frequency were made with a computer-aided circuit analysis. These estimates were found to be in good agreement with experimental measurements after initial adjustment of model parameters. The mechanism of excitation of the amplifier nonlinearity was identified as capacitor coupling between the amplifier metal case and critical sections of the printed-circuit etch as well as direct excitation via input circuits having little attenuation at radio frequencies.

PREFACE

This final report, covering the period September 1978 to November 1979, was prepared by CNR, Inc., of Needham, Massachusetts, under Contract No. F30602-78-C-0142 with the Rome Air Development Center, Griffiss Air Force Base, New York.

The CNR Project Engineer for the effort was Mr. J. W. Graham. Mr. C. J. Boardman performed the computer-aided circuit analyses. Mr. W. Welch carried out the difficult experimental effort with the assistance of Mr. D. Broccio.

The authors wish to acknowledge the support and assistance given by the Rome Air Development Center Project Engineer, Mr. D. Warren.

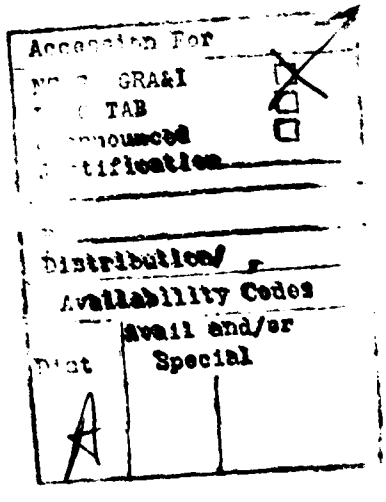

TABLE OF CONTENTS

Section		Page
1	INTRODUCTION AND SUMMARY	1-1
	1.1 Introduction	1-1
	1.2 Background	1-1
	1.3 Summary, Conclusions and Recommendations	1-2
2	THE RADIO FREQUENCY MODELING PROBLEM	2-1
	2.1 Objectives of the Modeling Effort	2-1
	2.2 A Case Study - Audio Circuit Modeling at RF Frequencies	2-2
	2.3 Description of the Audio Circuit	2-2
	2.4 Excitation of the Preamplifier by External Sources	2-7
	2.5 Devising a Practical Experimental Setup	2-7
	2.6 Excitation and Suppression of Undesired Modes	2-11
	2.7 Final Experimental Configuration	2-16
	2.8 The Possibility of Making Nodal Voltage Measurements within the Amplifier	2-16
3	DEVELOPMENT OF THE EQUIVALENT CIRCUIT MODEL	3-1
	3.1 Background	3-1
	3.2 Modeling the Amplifier in the HF, VHF, and UHF Regions	3-4
	3.3 Low- and Medium-Frequency Model - Normal Excitation	3-7
	3.4 Discussion of Circuit Model Parameters	3-10
	3.5 Modeling the Inductor L1	3-12
	3.6 Modeling the PC Etch and the Space between the Case Ground and External Ground	3-19
	3.7 Linear Model of the Amplifier and Test Circuit	3-23
	3.8 Comparison of Calculated and Experimental Linear Responses	3-26
	3.9 Further Comments	3-30

TABLE OF CONTENTS (Continued)

Section		Page
4	MODELING THE NONLINEAR RESPONSE TO AMPLITUDE-MODULATED EXCITATION	4-1
	4.1 Small-Signal Nonlinear Response to Amplitude-Modulated Signals	4-1
	4.1.1 Approximate Analysis - Power Series Model	4-1
	4.1.2 Second-Order Nonlinear Transfer Function Analysis	4-1
	4.1.3 Modeling the Nonlinear Amplifier	4-3
	4.1.4 Calculation of the Second-Order Nonlinear Transfer Function	4-5
	4.2 Measuring the Demodulated AM and Modeling the Spectrum Analyzer	4-7
	4.2.1 The Experimental Setup	4-7
	4.2.2 The Spectrum Analyzer Load	4-8
	4.2.3 Reducing Experimental Measurements to Obtain $\|H_2\|$	4-10
	4.3 Comparison of Predicted and Measured Second-Order Nonlinear Transfer Functions	4-11
	4.3.1 Normal Signal Input Excitation	4-11
	4.3.2 Case-Ground Input Excitation	4-13
	4.4 Discussion of the Nonlinear Model	4-15
	4.4.1 Normal Signal Input Nonlinear Model Frequency Dependence	4-15
	4.4.2 Case-Ground Input Nonlinear Model Frequency Dependence	4-15
	4.5 Using the Model to Predict an Equivalent Input to the Amplifier Caused by Nonlinear Distortion	4-19
	4.6 Comments on Amplifier Design Modification that will Reduce the Nonlinear Distortion	4-19

LIST OF TABLES

Table		Page
3-1	I/CAP Listing of Components for Low-Frequency Model	3-9
3-2	S-Parameters of Inductor L1 in Test Jig	3-17
3-3	I/CAP Listing of Equivalent Circuit Parameters	3-25

LIST OF ILLUSTRATIONS

Figure		Page
2.1	Sketch of Audio Amplifier showing Input and Output Cable and Ground Connections	2-3
2.2	Sketch of Audio Amplifier showing Approximate Layout	2-5
2.3	Schematic of Audio Amplifier	2-6
2.4	Excitation of Preamplifier Inputs by External Sources	2-8
2.5	Outline Sketch of Possible Experimental Configuration	2-10
2.6	Experimental Test Box for JFET Amplifier	2-12
2.7	Effective Load Network on the Input Cable	2-13
2.8	Equivalent Circuit at Input Cable Interface	2-15
2.9	Layout of Preamplifier showing Component and Cable Connection Detail	2-17
2.10	Cross Section of Preamplifier Test Fixture	2-18
2.11	Attempting to Measure a Voltage across an Arbitrary Node Pair	2-20
2.12	Typical Equivalent Circuits of Measurement Probes (Inner Mode)	2-21
3.1	Linear Model for JFET Audio Preamplifier for the HF/VHF Region	3-2
3.2	Amplitude Response of JFET Circuit Model	3-3
3.3	Amplitude and Phase Responses of JFET Amplifier after Model Parameter Adjustments	3-5
3.4	Low- and Medium-Frequency Equivalent Circuit Model of JFET Amplifier	3-8
3.5	Comparison of Predicted and Measured Voltage Gain (Magnitude) of the Low- and Medium-Frequency Model	3-11

LIST OF ILLUSTRATIONS (Continued)

Figure		Page
3.6	Inductor L1 as a Three-Terminal Network	3-14
3.7	Forward Transmission Loss of Inductor L1 in the Test Jig	3-15
3.8	Input Admittance of Inductor L1 in Test Jig	3-16
3.9	Comparison of Inductor L1 Model with Experimental Measurements	3-20
3.10	Symmetrical-T Model of Transmission Line	3-22
3.11	Linear Circuit Model of JFET Amplifier and Test Box for Frequencies less than 500 MHz	3-24
3.12	Case Ground Excitation Linear Response	3-27
3.13	SIG IN Excitation Linear Response	3-28
4.1	Power-Series Model - AM Excitation	4-2
4.2	Modeling the Nonlinear JFET Amplifier	4-4
4.3	Input Impedance of HP 3580A Spectrum Analyzer for 10- to 500-MHz Band	4-9
4.4	Second-Order Nonlinear Transfer Function for Normal Signal Input Excitation	4-12
4.5	Second-Order Nonlinear Transfer Function for Case-Ground Input Excitation	4-14
4.16	Input Circuits to Q1 for Normal Signal Input	4-16
4.17	Input Circuits to Q1 for Case-Ground Excitation	4-18

EVALUATION

The purpose of this effort was to develop a capability to model audio frequency circuits several orders of magnitude out of band. The motivation for this effort resulted from a previous attempt to model potential radio frequency (RF) effects on a system that operated within a narrow portion of the audio frequency (AF) spectrum. It was obvious that the behavior of the AF amplifiers could not be modeled by the components shown in the schematic drawings alone. The components and active devices had parasitic components such as the inductance and capacitance associated with their leads. The previous effort was able to satisfactorily model these effects up to about 70 MHz. The goal of the effort was to extend this modeling capability to 500 MHz, just below the microwave region. It was also hoped that it would be possible to measure the RF node voltages and branch currents within the circuit.

This effort demonstrated that it is possible to model AF circuits to a frequency of 500 MHz but to go beyond that limit appeared to be approaching the present realm of impossible. In order to push the limit this far it was not only necessary to model the parasitic components of the circuit elements but also those of the physical structure, in this case, the inductance of the printed circuit board etch as well as its capacitance to the circuit case. It is also important to model the associated measuring equipment at all frequencies of interest. An important conclusion drawn from this effort is that when significant discrepancies occur, check the model not the value of its components.

At this time it does not appear feasible to measure voltages and currents within the circuits because the measuring equipment will cause a serious purturbation of the circuit behavior, necessitating its modeling also.

This effort is considered to be a highly successful demonstration of the ability to model a circuit several orders of magnitude removed from its designed bandwidth (up to 500 MHz) provided that the model include the necessary parasitic and physical components and the characteristics of the measurement equipment. This was previously a missing link needed to model an entire electronics package outside of its designed operating bandwidth.

Daniel E. Warren

DANIEL E. WARREN
Project Engineer

SECTION 1

INTRODUCTION AND SUMMARY

1.1 Introduction

This report presents the results of an effort performed by CNR, Inc., of Needham, MA, for the Rome Air Development Center, AFSC, to further develop techniques for radio-frequency modeling of audio-frequency systems. The spectral region of concern is from near 0 to 500 MHz. The objective is to develop radio-frequency equivalent circuit models of audio systems that can be used with the assistance of computer-aided circuit analyses to predict the linear and nonlinear responses that would exist in the physical system. Techniques for experimentally determining the currents and/or voltages where physically possible are to be developed with emphasis upon model validation and the closely-related problem of parameter adjustment. It is desired to use the models to predict the effects of out-of-band interference such as amplitude-modulated radio carriers in generating nonlinear distortion products in the audio system output.

1.2 Background

There have been previous efforts to develop models of audio systems at radio frequencies. The principal relevant work is a previous effort to model an air-to-air missile control system amplifier that has been subjected to amplitude-modulated electromagnetic energy in the UHF aeronautical communications band between 225 and 400 MHz. This previous effort undertook to provide answers to several questions the most relevant of which is, "How are the UHF signals that are coupled to the circuit processed by the audio system?". Partial success was realized for frequencies below about 100 MHz by using equivalent radio-frequency models for discrete components in the system. It was recognized at the conclusion of this previous effort that much remained to be accomplished in understanding the mechanism of exciting the system nonlinearity and modeling its effects.

1.3 Summary, Conclusions and Recommendations

The approach employed has been to investigate the physical system from the missile application by using a test amplifier to guide understanding of the modeling problem and also to provide a vehicle for performing validation measurements. A review of the system application establishes that the amplifier can be conductively excited between its metal case and signal ground as well as at normal input or output terminals. An experimental configuration was devised to permit excitation of the amplifier in each of these modes. Special techniques were necessary to avoid excitation of indeterminate modes external to the amplifier. It was essential to suppress these modes to obtain valid measurements across the frequency spectrum to 500 MHz. A review of the possibilities of making measurements across internal node-pairs for purposes of obtaining information to adjust model parameters was made. It was concluded that such attempts would drastically upset the distribution of voltages within the physical circuit and excite indeterminate external modes unless such measurements were confined to 50 ohm impedances directly grounded to a good external ground plane. It was also recognized that measurements of low-frequency nonlinear distortion required a high input-impedance audio instrument at the amplifier output. The impedance of this instrument must be modeled across the entire radio-frequency band. In developing a detailed model for the 500 MHz bandwidth, it was necessary to model the printed-circuit board etch as cascaded symmetrical-T sections. The amplifier is a tuned amplifier with a large shielded-inductor in the parallel-resonant load at the amplifier output. It was necessary to devise a wideband radio-frequency model of the inductor including the effects of the shield. The linear model of the amplifier for frequencies to 500 MHz was terminated in 50 ohm loads and predictions were made of transmission through the amplifier for both normal signal input and case ground excitation. These predictions were compared with measurements made on the test amplifier. It is shown that over most of the frequency range from 1 - 500 MHz, the linear coupling through the amplifier for case-ground excitation exceeds that for normal signal input by a substantial margin. It is also found that above 10 MHz, the gain of the active device (a JFET) in the amplifier plays no significant role in determining the coupling to the output.

After expressing the audio output of the amplifier for amplitude-modulated excitation in terms of second-order nonlinear transfer functions, a detailed model is derived that permits calculation of the detected output in terms of the linear response from the excitation port to the site of the nonlinearity in the JFET and the gain of the amplifier at its audio-tuned frequency. The gain to the JFET nonlinearity is calculated by computer-aided analysis of the wideband radio frequency model of the amplifier with a wideband model of an audio spectrum analyzer at the amplifier output. Measurements of detected output are compared with the model prediction and shown to be in good agreement across the frequency spectrum from 50 kHz to 500 MHz.

It is concluded that the techniques developed, including the methods of analysis and modeling, have been validated by the measurement effort. Recommendations regarding model improvement are commented upon in the text. It would be highly desirable to have a computer-aided circuit analysis program that would permit introduction of mathematically-computed impedances or impedances derived from experimental data at arbitrary branches in the high-frequency model. It is not possible to model some of the important physical elements in the system by lumped R, L, or C components. This is particularly true for wideband models of ferrite-core inductors, transmission-line models of printed-circuit etch, and wideband models of instrumentation that must be connected to the amplifier in order to perform measurements. Experience in developing the wideband model of the amplifier also firmly convinces one that it is necessary to have a good idea of the physical layout and arrangement of components and etch including the details of shielding and possible sources of excitation before one can expect much. If the model prediction fails to agree reasonably with measurements, it is often not the parameter values of the model that are the problem but the model itself. Physically significant effects have probably been omitted. Close physical examination of the amplifier aids greatly in improving the model.

Insofar as the mechanism for exciting the nonlinearity in the test amplifier is concerned, it is very apparent what is happening. For normal signal input excitation, the amplifier has no attenuation before the nonlinearity whatsoever

below 1 MHz. Above 1 MHz, the coupling to the nonlinearity gradually reduces by about 20 dB at 100 MHz, at which point no further significant reduction occurs. For case-ground excitation, the excitation of the nonlinearity is caused by capacitance coupling between the amplifier metal case and the printed-circuit signal etch at or near the physical location of the field-effect transistor. The signficant coupling capacitances are only a few tenths of picofarads, but they are very critical.

SECTION 2

THE RADIO FREQUENCY MODELING PROBLEM

2.1 Objectives of the Modeling Effort

Our objective has been to develop experimental techniques and electronic circuit models of audio-frequency circuits that have been excited by radio frequency energy at frequencies up to 500 MHz. In particular, we are interested in the prediction of undesired nonlinear responses of an audio circuit to amplitude modulated RF excitation generated by undesired RF radiation sources coupling to the circuit. The coupling mechanism of concern is not direct radiation pickup in the circuit itself but, instead, pickup in the external cabling, grounds, and loads to and from the audio circuit. The circuit is assumed to be shielded from direct radiation pickup. Thus, excitation of the circuit is via its terminals, including grounds and shield connections. The electromagnetic interference (EMI) is, therefore, conducted interference insofar as the audio circuit is concerned.

Note that modeling EMI radiation pickup in connecting cables and grounds plays a direct part in establishing the excitation levels of the audio circuit in terms of incident electromagnetic field strengths. Also, the physical layout and arrangement of the connecting cables and grounds plays a direct role in determining: (1) the source impedances through which external excitation must couple to the circuit; and (2) the load impedances attached externally to the circuit. These external impedances are very significant in determining the circuit response to EMI. They also lead to many experimental problems and considerable difficulty in devising meaningful experimental measurements. Unless a carefully controlled experiment configuration can be devised without indeterminate or uncontrolled terminating impedances, it becomes impossible to validate model estimates by comparison with experimental measurements.

Others have been concerned with the excitation of the external cables, grounds, and leads. It is not within the scope of our study to pursue such matters. Yet, the problem will not go away so nicely by just ruling it beyond scope. We will, when

necessary, concern ourselves with such matters, but only to the extent that we may understand the probable mechanism of exciting the audio circuit and avoiding those difficulties referred to above that are associated with attempts to perform experimental measurements for purposes of validation.

2.2 A Case Study - Audio Circuit Modeling at RF Frequencies

As is frequently the situation in problems of the sort we are investigating, it is desirable to have a physical example at hand to guide understanding of the modeling problem and to provide a vehicle for trying out models and performing measurements. In other words, we have a "case" to study. Experience shows that when one encounters difficulties with a model prediction that does not seem to agree with physical measurements, it is not often the parameters of the model that are the real problem; but, instead, some not-so-obvious physical mechanism is present in the physical circuit and it has been completely omitted in the model. No amount of parameter adjustment remedies this difficulty unless one attempts to model with generalized mathematical models endowed with handfulls of parameters that all need values but have no physical counterpart in the circuit from which to estimate a parameter value. One is reduced to curve fitting by adjusting the parameters to fit measurements, but no physical significance can be associated with the model or its parameters so determined. Since the objective is to construct a model from which performance can be predicted rather than having a measured performance and fitting a model to it, we shall try to avoid model elements that do not have a direct physical counterpart in the circuit.

2.3 Description of the Audio Circuit

Figure 2.1 shows a sketch of the audio preamplifier we shall use as a vehicle for our investigation. The amplifier is a tuned audio amplifier with a voltage gain of approximately 27 dB at its tuned frequency of approximately 1200 Hz. Low-level inputs to the amplifier couple from the sensor cell through a short length of coax cable to terminal board TB1 with the center conductor wired to SIG IN and the outer conductor connected to SIG GND. The amplifier is enclosed within a shielded case that has physical contact with a relatively large external ground plane. The supporting structure for the sensor cell and its relationship to the external ground is ambiguous. The input cable is, however, approximately 23 cm in length which, we note, is approximately a quarter-wavelength at 300 MHz. The output

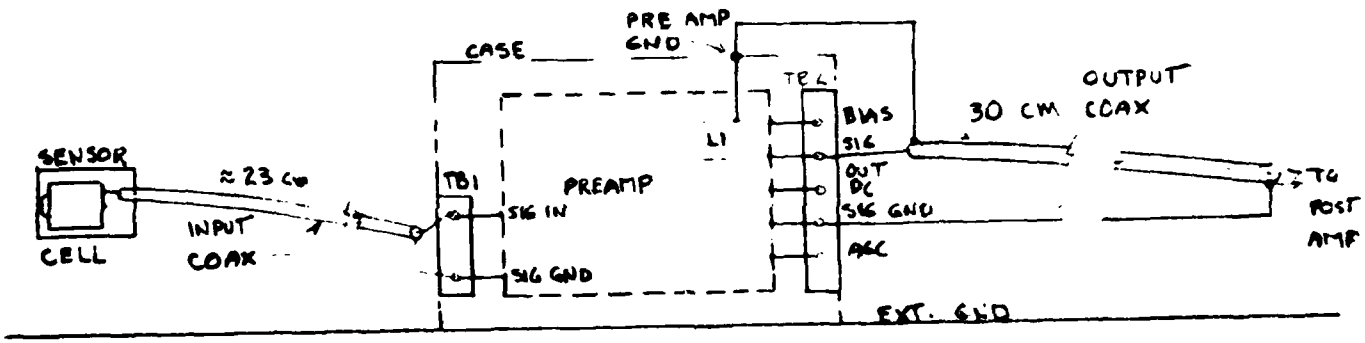

Figure 2.1 Sketch of Audio Amplifier showing Input and Output Cable and Ground Connections

coax cable has its center conductor wired to SIG OUT on TB2, but the outer conductor is connected to PREAMP GND which is the amplifier metal case. The amplifier SIG GND connects by an independent wire to the outer coax conductor at the postamplifier load end. This arrangement is evidently an attempt to surround the SIG OUT lead by a shield to avoid electrostatic pickup. The output wires are also more than a quarter-wavelength long at 300 MHz. As we shall see shortly, the SIG GND terminals, which are common at input and output, do not physically connect to the case ground (PREAMP GND). There is also an inductor L1 in the preamplifier that has a shielding case that is also connected directly to the preamplifier metal case, but not to the SIG GND terminal. Figure 2.2 shows an additional sketch of the preamplifier with further physical detail. Note that the output end (TB2) of the case is open but essentially physically obstructed by the inductor case. The amplifier electrical components, which are all discrete components, are mounted on the top side of the printed circuit (PC) board in a conventional manner with leads passing through the board and soldered to the PC etch on the lower side of the board. A thin dielectric spacer insulates the PC etch and somewhat projecting component leads and solder from contact with the bottom of the case. Leads inside the case from TB1 and TB2, which are relatively short open wires arranged without particular concern, pass through the PC board from the top, and are soldered on the lower side at appropriate locations.

A schematic diagram of the amplifier is shown in Figure 2.3. Transistor Q1 is a discrete component JFET providing the active gain in the circuit. Observe that the amplifier input impedance at audio frequencies is approximately 500 kilohms. Capacitance C2 is sufficiently large that signal components at the amplifier tuned frequency of 1200 Hz are passed without significant attenuation. The parallel-resonant tuned circuit consisting of C3 ($\approx$ 2200 $\mu\mu$f) and L1 ($\approx$ 7.4 henries) with bandwidth set by the damping resistance R6 ($\approx$ 150K ohms) constitutes the tuned impedance in the JFET drain circuit. The external load impedance at audio frequencies between the output SIG OUT and SIG GND is high ($>$ 500K ohms).

The gain of the amplifier is adjustable by varying the voltage applied to the AGC input to the gate of Transistor Q2. Q2 is also a JFET. Adjusting the gate voltage of Q2 changes the incremental resistance between the drain and source of Q2. This resistance change varies the amount of negative feedback between the source of Q1 and SIG GND, thereby adjusting the amplifier gain. Throughout our modeling we shall assume that

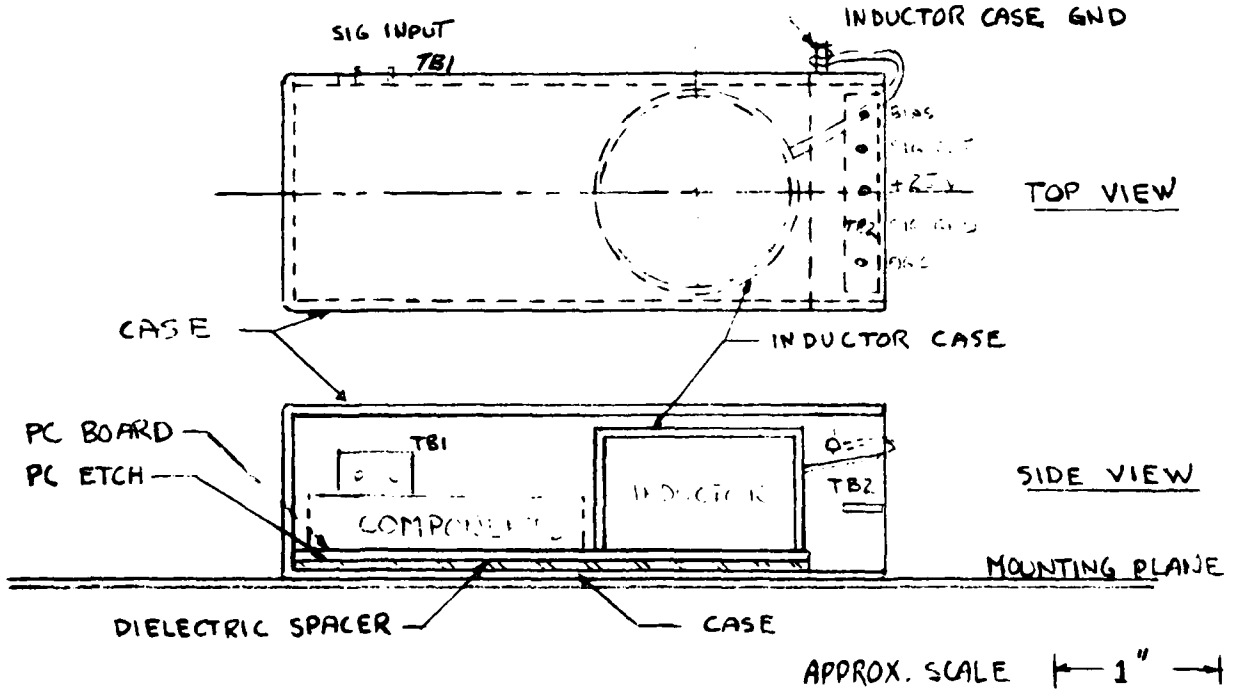

Figure 2.2 Sketch of Audio Amplifier showing Approximate Layout

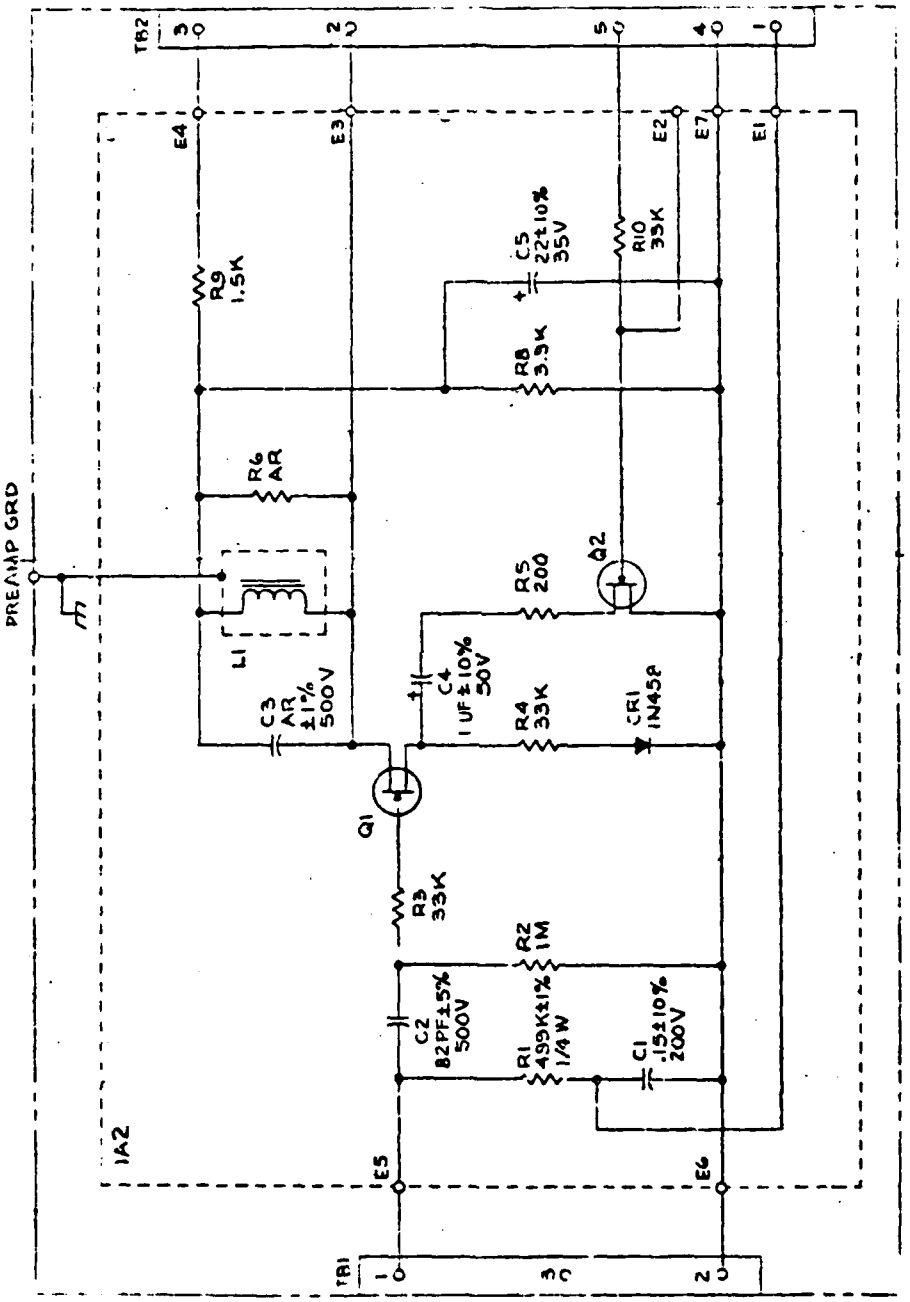

Figure 2.3 Schematic of Audio Amplifier

the AGC input to the gate of Q2 has been grounded to SIG GND. Note that the +25 voltage power supply voltage is delivered to Q1 across the voltage divider resistances R9 and R8 with C5 bypassing the midpoint to provide a good audio low impedance to SIG GND.

2.4 Excitation of the Preamplifier by External Sources

Figure 2.4 illustrates approximately the external region at the interface input to the preamplifier. Desired signals near 1200 Hz originate in the sensor cell and propagate to the amplifier input through the input coax to SIG IN and SIG GND. The external region also is immersed in the EMI radiation field which we assume can have carrier frequencies as high as 500 MHz. Therefore, the outer conductor of the coax is excited in a significant manner by undesired signals. Some of this signal will couple via the sensor cell through the coax into the normal signal excitation ports. Also, a significant portion of this interference will also appear at the SIG GND - CASE input to the preamplifier by propagating in the region between the coax outer conductor and external ground directly into the preamplifier between the SIG GND and CASE ground region. Note that the uncertain coupling between sensor cell and ground plane, denoted by the question mark, will have an impact upon this signal but will not eliminate the coupling even if it were a very low impedance. We observe, therefore, that any attempt at realistic modeling of the amplifier at frequencies as high as 500 MHz must include the possibility of excitation between the CASE and SIG GND.

Circumstances at the output terminals of the preamplifier are much the same as the input.

2.5 Devising a Practical Experimental Setup

Much effort was devoted to devising a practical experimental setup that would permit repeatable measurements of both linear and nonlinear responses of the preamplifier for both excitation of the normal signal input and the case ground. Successful resolution of this difficult problem was essential if there was to be any chance of obtaining experimental measurements to obtain data for comparison with model predictions. Indications of the measurement difficulties, particularly in the 50 - 500 MHz spectral region, were obtained by several early attempts to make linear transmission measurements through the

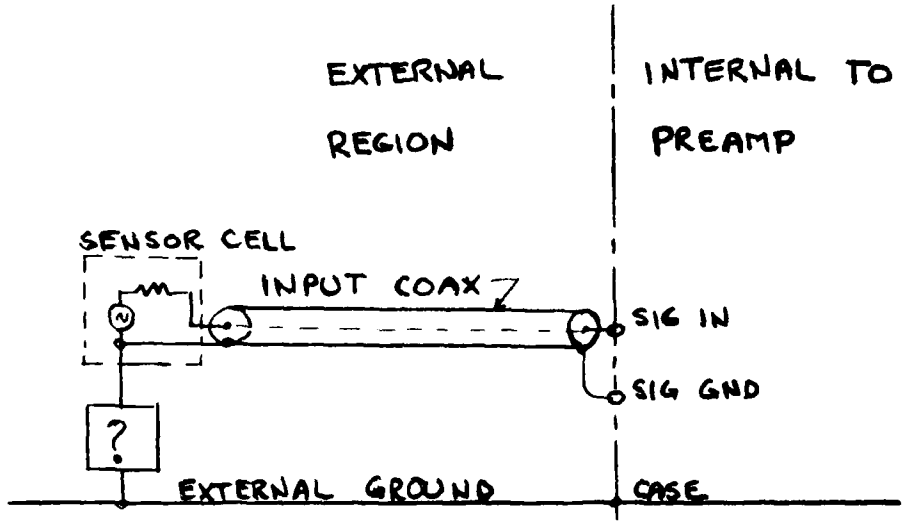

Figure 2.4 Excitation of Preamplifier Inputs by External Sources

amplifier. The amplifier printed circuit board with all components was removed from the metal case. This was done for several reasons. First, the arrangement of input and output leads inside the case between the terminal boards TB1 and TB2 and the PC board was indeterminant and had to be controlled in a known manner if model verification was to be expected. Second, it was originally anticipated that access would be needed to individual nodes throughout the PC board to assist in adjusting model parameters based upon nodal voltages. It was also recognized that the circuit would need to be frequently inspected physically to aid in the model development. Also, it was recognized that the part of the case that must be present in the experimental model was that part in close proximity to the PC etch underneath the board rather than the rest of the surrounding case since experimental measurements would be made with signal sources coupled by cables directly to the terminals of the amplifier rather than by immersing the amplifier into a radiation field where the shield would be necessary.

Figure 2.5 shows an outline sketch of a possible experimental configuration. The "case ground" is a conducting metal sheet separated from the PC circuit board by the actual dielectric spacer from the amplifier referred to previously. Note the indicator case connected to the case ground.

The grounding of input and output connecting cables had to be examined with much care. It was mandatory that the input signal cables and output measurement instruments have a common ground. A network analyzer was used for linear transmission measurements. The instrument has common grounds at input and output. It was also mandatory that the nonlinear response from the amplifier (at $\approx$ 1200 Hz) be measured at the normal signal output terminals with the output cable grounded to the SIG OUT terminal, as shown in Figure 2.5. Also, as shown in Figure 2.5, "case ground" excitation of the amplifier could be accomplished by shifting the input coax conductor from the normal SIG IN on the PC board to the "case ground" without disturbing the coax outer conductor connections to SIG GND. It was <u>not</u> permissible to ground the case ground plane to the external ground plane and, thereby, remove the open region between the case ground and external ground from the experimental setup. "Case ground" must be kept as an independent input. If it were grounded to the external ground, a direct short would be placed across the input signal when "case ground" excitation was desired since the instrumentation at the signal source and at

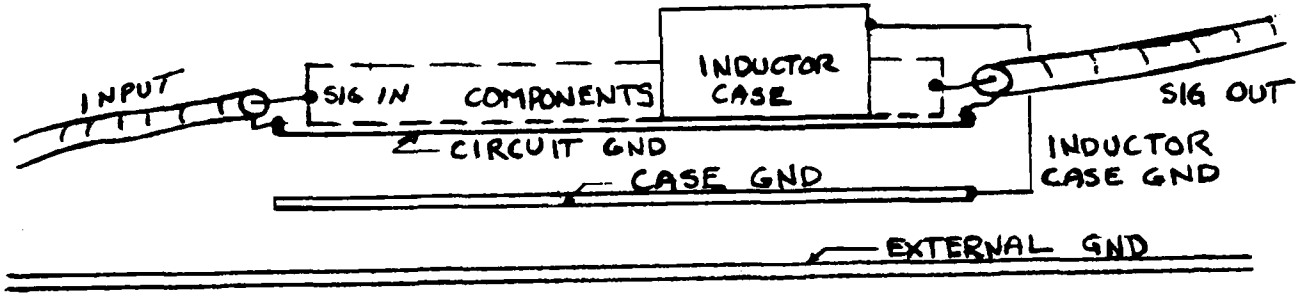

Figure 2.5 Outline Sketch of Possible Experimental Configuration

the measurement end of the signal output coax all share a common ground through the external ground plane. Therefore, an insulating dielectric spacer is also required between the case ground and external ground plane. The effects of this region must be accounted for in the model.

Figure 2.6 shows the JFET amplifier placed inside a metal box enclosure with connecting coax cables attached to bulkhead coax connectors at the side of the box. This provided a fixed arrangement for the cables inside the box relative to the amplifier and metal ground plane (the box). The placement of instruments and cables external to the box then becomes noncritical. Provision was also made to completely cover the box with an RF tight cover should problems be experienced with high field strength local TV and FM radio stations in the laboratory vicinity. This step proved ultimately not to be necessary primarily because the entire setup was moved inside an RF shielded room when difficulties of this nature were anticipated.

2.6 Excitation and Suppression of Undesired Modes

When the preamplifier configuration described in Section 2.5 was set up and measurements of linear transmission responses through the amplifier terminals attempted, the results were most discouraging. The metal box, with its interior cables, was being excited by the amplifier in a very undesirable manner. These effects were most evident in the 50 - 500 MHz spectral region. Grounding the "case ground" to the bottom of the box only changed the details of the excitation but did not reduce or eliminate it. Transmission gain through the box was effected by placing one's hand in the vicinity of the cables and amplifier. If a cable outer conductor was touched, many tens of dB changes in gain would occur with drastic frequency shifts in the nulls and peaks in the gain across the band. Clearly, the outer conductor of cables was supporting standing waves, and they would have to be eliminated before reliable data could be obtained.

Figure 2.7 illustrates the mechanism of excitation of a cable outer conductor from a circuit point-of-view. The input cable is shown connected to the SIG IN and CKT GND (SIG GND) normal connection. Nodes "CASE GND" and "EXT GND" are shown. Impedances Z1, Z2, and Z3 are effective impedances connecting the nodes SIG IN, CKT GND, and CASE GND internal to the amplifier. Z4 is the impedance between the case ground plane and the external ground plane. Z_{out} is the effective input impedance

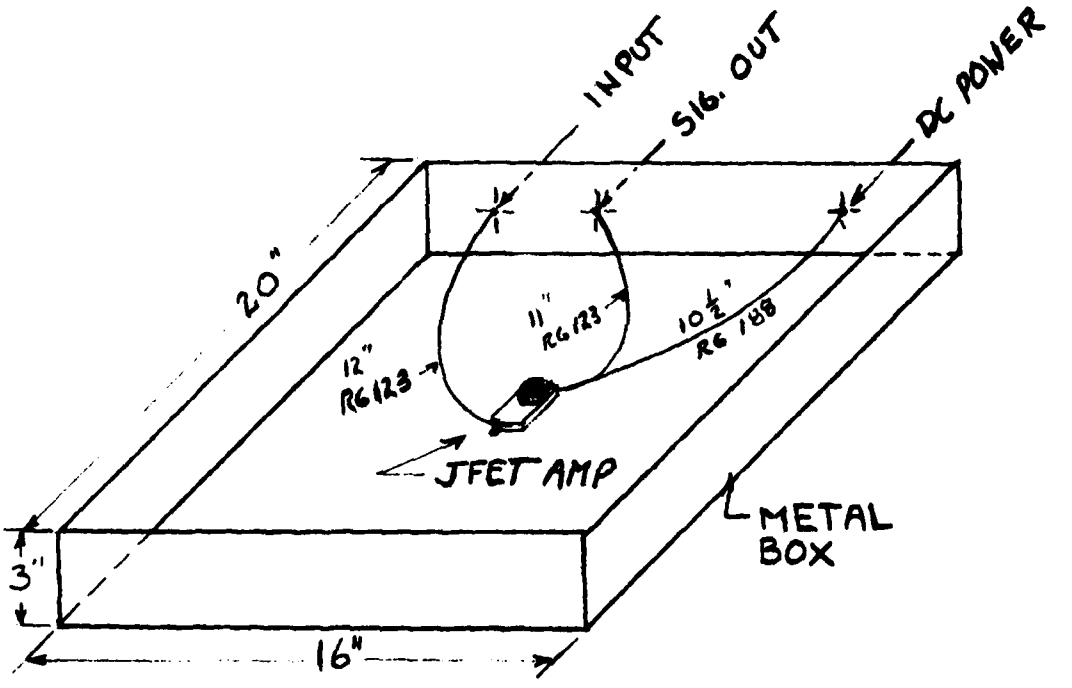

Figure 2.6 Experimental Test Box for JFET Amplifier

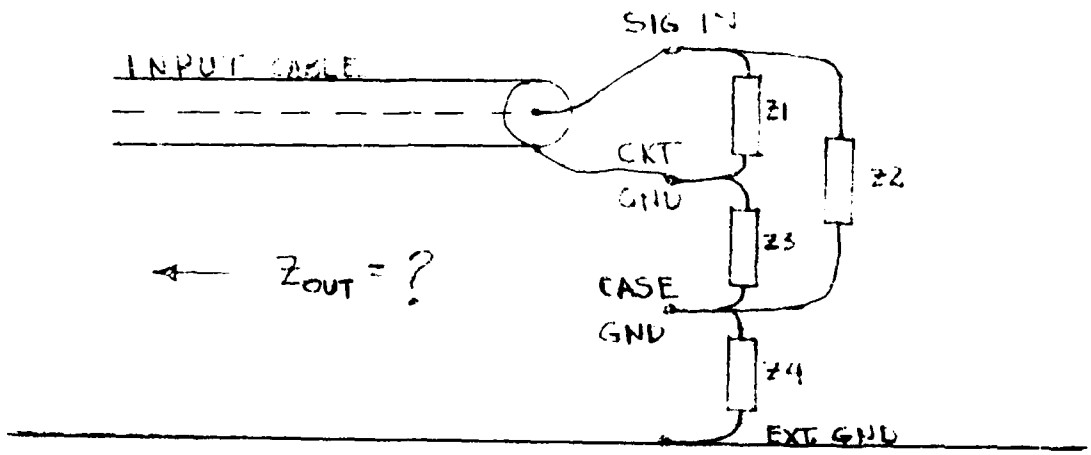

Figure 2.7 Effective Load Network on the Input Cable

at the amplifier interface between the input cable outer conductor and the external ground plane looking back toward the origin of the input cable. At low frequencies, this impedance is low since the outer conductor is grounded to the metal box at the bulkhead connector where the signal passes through the side of the box. From the point-of-view of the amplifier terminals, Z_{out} is simply the input impedance of a nonuniform transmission line having a short circuit at its far end which, from Figure 2.6, is about 12 inches away. Shorting the "case ground" node to the external ground does not alter Z_{out} but simply shorts out Z4 in Figure 2.7.

Figure 2.8 shows an alternative equivalent circuit at the cable interface with the input cable shown as a signal generator with source impedance Z_G. Impedance Z_{out} represents the unwanted mode. Any voltage across, or current through, Z_{out} means that the mode is excited. To eliminate this mode, it is necessary to do one of the following:

(1) Open circuit Z2. This is impossible since there are extensive regions throughout the PC board in very close proximity to the case ground.

(2) Open circuit Z4. The amplifier must be physically supported. The region between the case ground plane and the external ground is an enclosed volume that can be viewed as a parallel-plate transmission line with known geometry and dielectric. At best it is a capacitance; at worst it is a transmission line bypass between the input and output sides of the amplifier. It cannot be open-circuited.

(3) Short circuit Z3. Excitation of the CASE GND node relative to the CKT GN (SIG GND) node is one of the main entry points for external EMI into the amplifier. Z3 cannot be shorted since we specifically wish to investigate matters when it is not shorted.

(4) Short circuit Z_{out}. Shorting Z_{out} by strapping the circuit ground directly to the external ground is an acceptable method for suppressing the undesired excitation of the input cable outer conductor. When Z_{out} is shorted, Z4 and Z3 are placed in parallel. Inputs at both SIG IN and CASE GND will excite the Z4 region between the case ground and external ground plane. Therefore, any modeling of the amplifier must include an accurate model of the Z4 region.

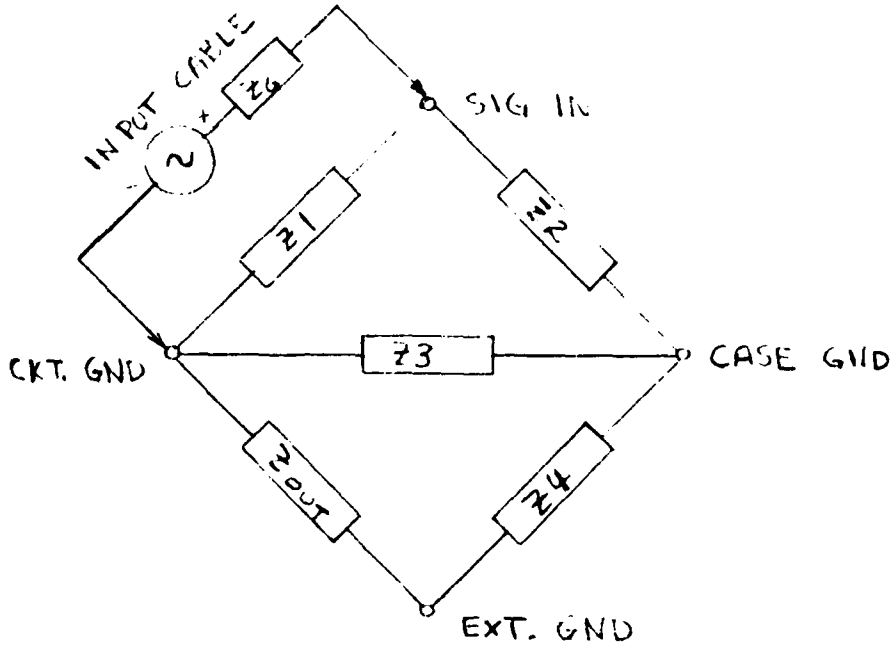

Figure 2.8 Equivalent Circuit at Input Cable Interface

It was also observed experimentally that the outer conductors of the signal output coax cable and dc power coax cable are excited by the amplifier at the output interface. These undesired modes are also suppressable by strapping the output SIG GND terminal to the external ground plane.

2.7 Final Experimental Configuration

Figure 2.9 shows a layout of the preamplifier test fixture with the mode-suppressing ground straps in place at the amplifier input and output terminals. Also shown in the diagram is the layout of the electronic components in the amplifier and the layout of the PC etch. Note that the case ground plane extends beyond the printed circuit board and that the inductor L1 case is grounded to the case ground in two places with the center of the grounding wire soldered to the side of the inductor case. Figure 2.10 shows further detail in the form of a cross section through the PC board, the case ground, and external test box grounds with separating dielectric spacers illustrated. Note the grounding straps.

The input cable (see Figure 2.9) was connected to the SIG IN terminal for "Normal Excitation" of the amplifier. For "Case Ground Excitation", the center conductor was moved to the adjacent case ground input terminal located on the case ground plane. This provided a very simple means for changing between the two inputs to the amplifier without any further disturbance to the configuration either inside or outside the test setup.

The ground-strap mode suppressors were quite effective in eliminating the excitation of the connecting-cable outer conductors. Transmission measurements through the setup were repeatable with only small disturbances above 400 MHz associated with incomplete suppression of fields near the cable/amplifier interface. Once these results were obtained, it was determined that reliable measurements were then obtainable and that the modeling effort could proceed with reasonable prospects of including within the entire model those parts of the experimental setup that were necessary to have a reliable experimental measurement.

2.8 The Possibility of Making Nodal Voltage Measurements within the Amplifier

As suggested previously in Section 2.5, it was originally anticipated that knowledge of voltages across individual node

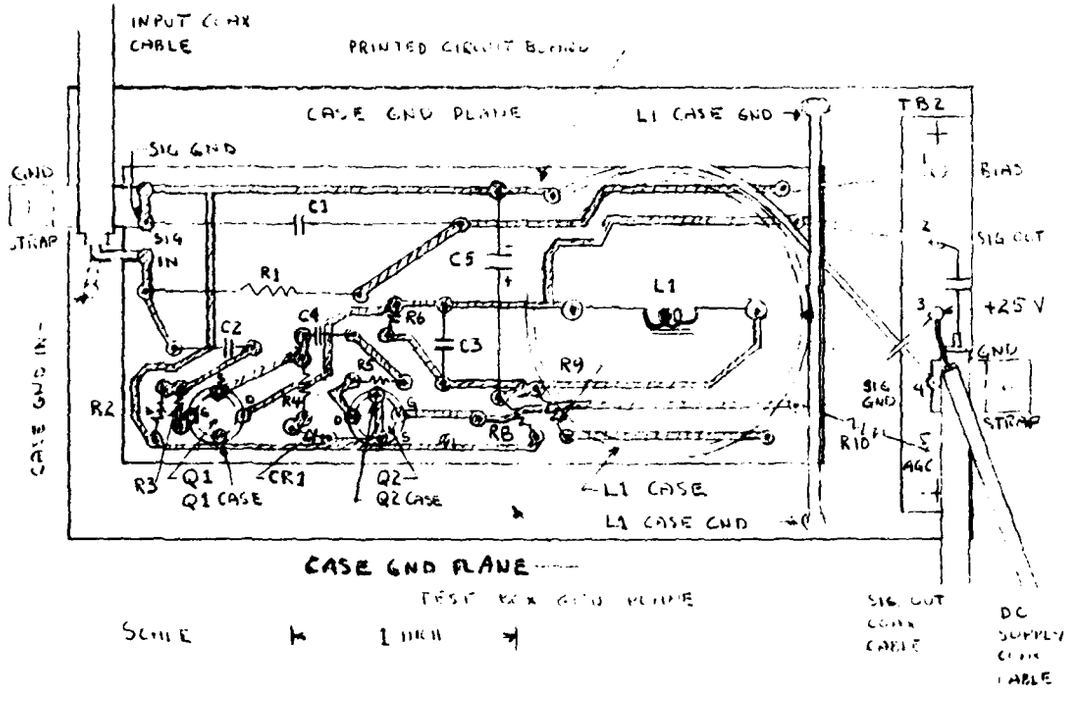

Figure 2.9 Layout of Preamplifier showing Component and Cable Connection Detail

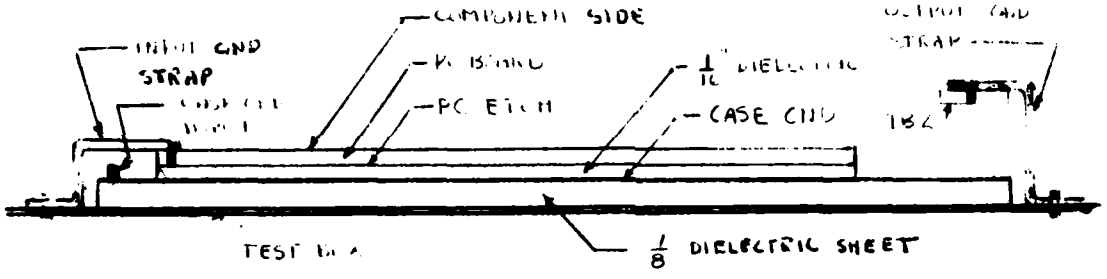

Figure 2.10 Cross Section of Preamplifier Test Fixture

pairs within the amplifier circuit would provide information that would assist in adjusting the parameters of equivalent circuit models. This can be demonstrated to be a false hope because of significant experimental difficulties. Consider the situation illustrated in Figure 2.11. As we have seen previously, we have an amplifier with several different "ground" nodes. Only the external ground plane in the experimental test configuration is a common ground reference throughout the test fixture. All other grounds are just other nodes that have voltages relative to the common ground that depend upon the circumstances. In the figure we illustrate an attempt to measure a voltage across a node pair connected by impedance Z2. These nodes have impedances Z1 and Z3, respectively, with respect to the common external ground node. Ideally, we would wish the measurement probe (assumed unbalanced) to have an inner-mode impedance Z_{inner} and outer-mode impedance Z_{outer} to be sufficiently large that neither the inner nor outer modes would disturb the distribution of currents and voltages within the circuit when the probe is attached to the node pair in question. Figure 2.12 illustrates typical equivalent circuits for the inner mode of both high and low impedance probes. The broadband probes have low impedances making them suitable only for use in a 50-ohm environment. The so-called high-impedance probes are much too narrowband. They are also of not sufficiently high impedance to avoid a major upset of the amplifier circuit involved. We shall see later that the capacitive coupling between the PC etch and the case ground plays a very dominant role in determining the VHF and UHF distribution of voltage and currents within the network. The typical probe capacitance of 2.0 - 2.5 pf is of the same order or greater than the PC etch capacitances. Hence, there is no doubt regarding the impact of a probe in upsetting the voltage distribution within the circuit.

The probe outer-mode impedance (see Figure 2.11) is indeterminant. It depends upon the location of the leads to the measurement instrument in much the same manner as the excitation of the outer conductor of the input cable did. The impedance will vary from high to low and be highly frequency-dependent with resonant spacing dependent upon lead lengths. To avoid this intolerable situation, we must obstruct excitation of the outer mode by grounding the probe low side directly to the external ground. Therefore, only node voltage measurements relative to the common ground reference plane can be attempted.

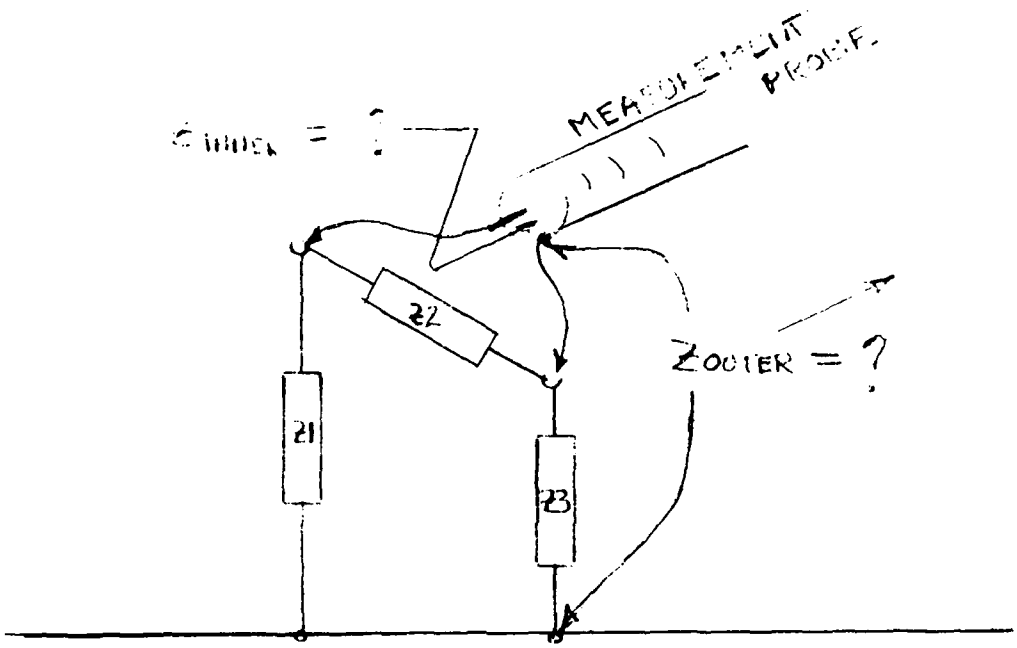

Figure 2.11 Attempting to Measure a Voltage across an Arbitrary Node Pair

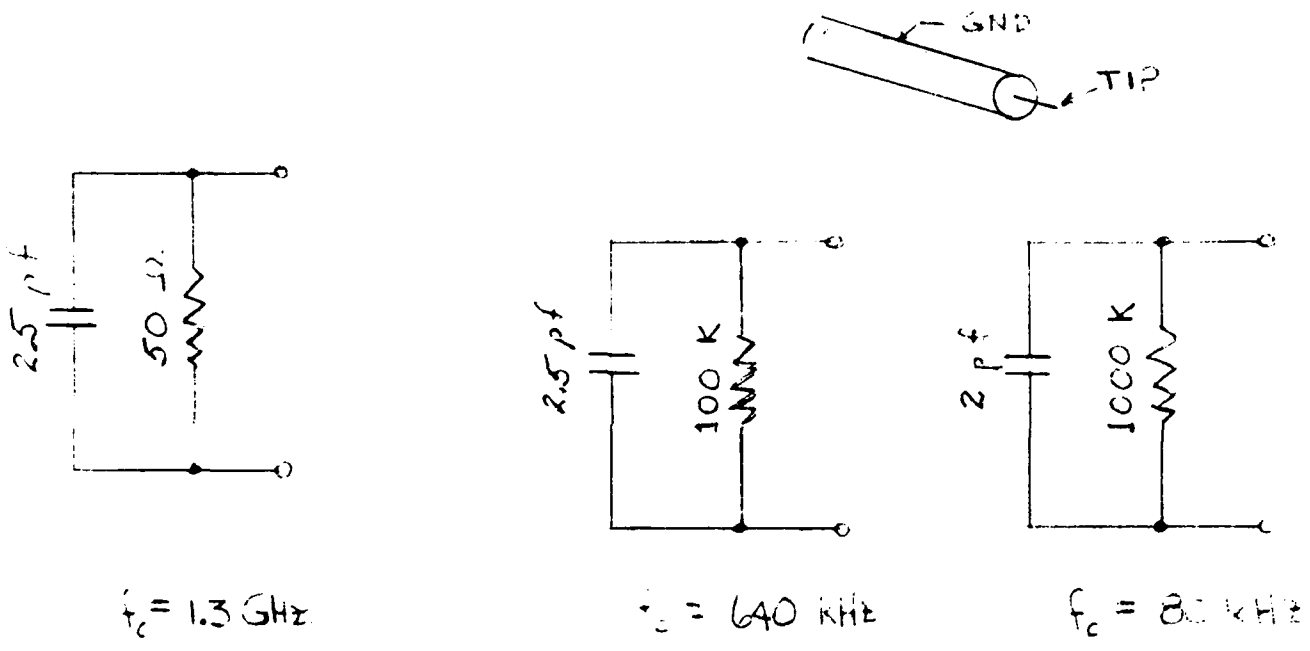

Figure 2.12 Typical Equivalent Circuits of Measurement Probes (Inner Mode)

The conclusion follows that, for all practical purposes, when we are concerned with spectral regions up to 500 MHz, we must limit node voltage measurements to 50-ohm impedance levels and to make these measurements with respect to the external ground plane. This directly implies that we must confine measurements to transmission measurements through the amplifier at the amplifier terminals and be prepared to include the 50-ohm model of the probe in any equivalent circuit model. We shall see that we just as well can use a network analyzer for linear measurements. Special precautions are necessary when we are after the nonlinear responses. For example, the normal load impedance on the SIG OUT terminal at low frequencies is greater than 500 kilohms. Therefore, it is necessary to use high impedance instruments to make measurements of the nonlinear response at 1200 Hz caused by nonlinear detection of amplitude-modulated radio frequency signals exciting the amplifier. A low-frequency spectrum analyzer having good resolution and sensitivity was found to be necessary. Although the input impedance of the spectrum analyzer was high at low frequencies, its input impedance at radio frequencies was not high and had to be measured and added to the model as transformed by the coax cable between the test fixture and the spectrum analyzer. In other words, it is necessary to include the broadband input impedance of low-frequency measurement instrumentation to adequately account for nonlinear responses since the high-frequency impedances impact the excitation of the nonlinearity.

SECTION 3

DEVELOPMENT OF THE EQUIVALENT CIRCUIT MODEL

3.1 Background

There have been earlier efforts to model the JFET audio amplifier described in the previous section. The amplifier design has served as a convenient vehicle for the development of HF and VHF circuit models of audio frequency circuits. Of particular value is the work described by Whalen and Paludi in their paper published in 1977 in the International Journal of Electronics [3.1]. The objective of Whalen and Paludi's paper was to point out the need to include component parasitic elements in the models of circuit components if one wished to account for the performance of audio-frequency circuits in the HF/VHF region. Their results provide a starting point for our circuit model. Figure 3.1 shows the linear equivalent circuit of the audio-frequency JFET amplifier used for their analysis in the HF/VHF region. The elements inside the dashed lines are the component parasitic elements. The circuit models inside the solid lines are the solid-state semiconductor circuit models. Reference to Figure 2.3, the schematic diagram of the amplifier, will be helpful in understanding Figure 3.1. Node 2 is the SIG IN terminal. Node 10 is the SIG OUT terminal with capacitance C6 added as a dc blocking element to permit the connection of the 50-ohm low impedance external test equipment. The arrangement of 50-ohm resistances at the input terminal is a model of the signal source employed in the measurement of the circuit response.

Whalen and Paludi do not address the grounding and case excitation issues we have raised in Section 2.6. It can be assumed that they have avoided introducing these complications by shorting the SIG GND, CASE GND, and any external grounds together at both the amplifier input and output. Figure 3.2 shows Whalen and Paludi's computer-aided circuit analysis results for the three different sets of parasitic component values listed in the table also in Figure 3.2. They point out that the parasitic capacitance CR3 in parallel with R3 (33 kilohms) is critical and that the parasitic inductances LC3 and LC5 series resonate with capacitance C3 to produce the deep null in the response near 25 MHz.

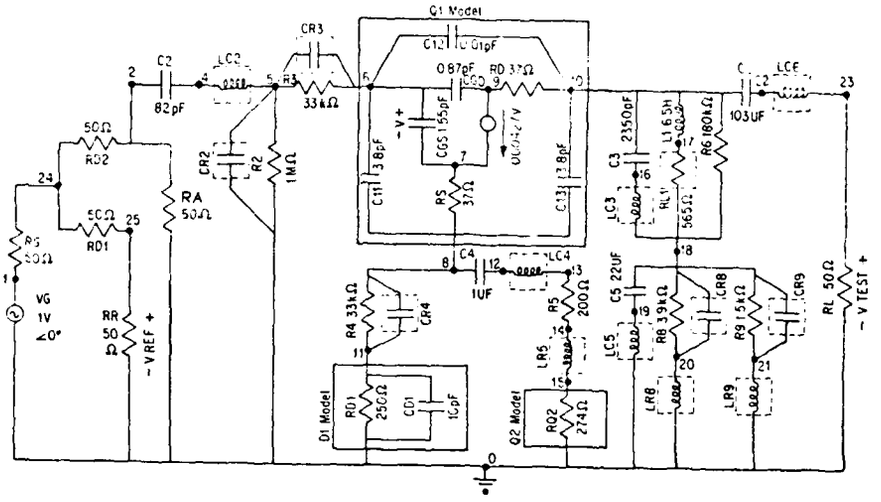

Figure 3.1 Linear Model for JFET Audio Preamplifier for the HF/VHF Region (taken from [3.1])

Simulation	(1)	(2)	(3)
LC2	0·1 nH	10 nH	10 nH
LC3	0·1 nH	10 nH	10 nH
LC4	0·1 nH	10 nH	10 nH
LC5	0·1 nH	10 nH	10 nH
LC6	0·1 nH	10 nH	10 nH
LR5	0·1 nH	25 nH	25 nH
LR8	0·1 nH	25 nH	25 nH
LR9	0·1 nH	25 nH	25 nH
CR2	0·01 pF	0·2 pF	0·4 pF
CR3	0·01 pF	0·2 pF	0·4 pF
CR4	0·01 pF	0·2 pF	0·4 pF
CR8	0·01 pF	0·2 pF	0·4 pF
CR9	0·01 pF	0·2 pF	0·4 pF

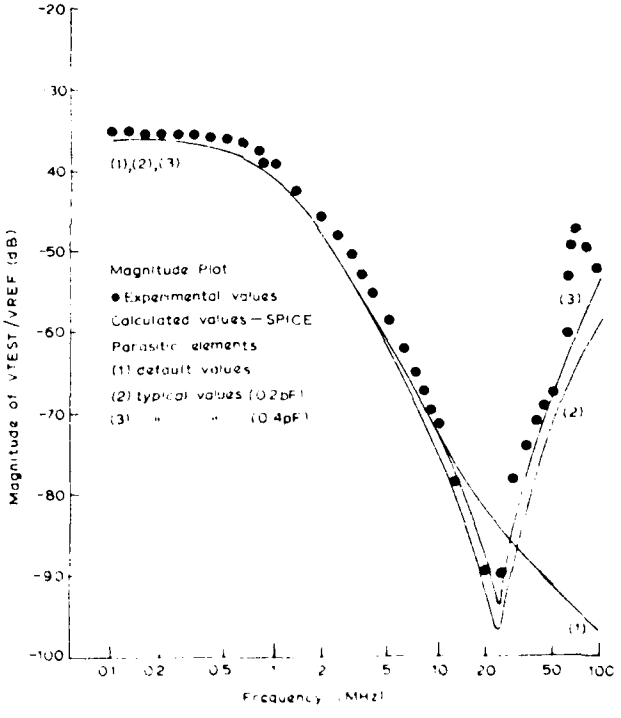

Figure 3.2 Amplitude Response of JFET Circuit Model (taken from [3.1])

Whalen and Paludi subsequently undertook to improve their circuit model by taking additional measurements and by adjusting circuit parasitic elements to better fit the measured results. Figure 3.3 shows the results of this effort. Parasitic element values were those from Simulation 3 (Figure 3.2) with the following changes: LC3 = LC5 = 13 nH; RC5 = 0.2 ohm, C11 = C13 = 0.5 pF; RS = RD = 27 ohms. These results are generally in good agreement with measurements at frequencies below 25 MHz. Whalen and Paludi attribute the deviations above 25 MHz to capacitive and inductive effects associated with the PC board.

3.2 Modeling the Amplifier in the HF, VHF, and UHF Regions

Whalen and Paludi's model provides a good HF (3 - 30 MHz) region starting point, but there are many changes that had to be made to begin to adequately account for the amplifier performance in a realistic excitation and loading environment over frequencies up to 500 MHz. The following comments are pertinent:

(1) Excite the Case Ground as well as Normal Input

In addition to excitation at the SIG IN terminal, we must also account for excitation at the case ground. In fact, insofar as the linear response of the amplifier is concerned, the output response for case excitation significantly exceeds the normal input response throughout the 1 - 500 MHz region!

(2) 50-Ohm Loads down the Amplifier

The assumption of a 50-ohm output load is an experimental convenience necessary to permit making linear output measurements in the spectral regions of interest. The presence of such a low-impedance loads down the output circuit to such an extent that the performance of the model becomes nearly independent of the Q1 JFET drain parallel elements to signal ground.

(3) Audio Load Must Have a Broadband Model

The primary (and ultimate) objective is to model the nonlinear response of the amplifier to electromagnetic interference conductively-coupled to the amplifier via the signal and case ground inputs.

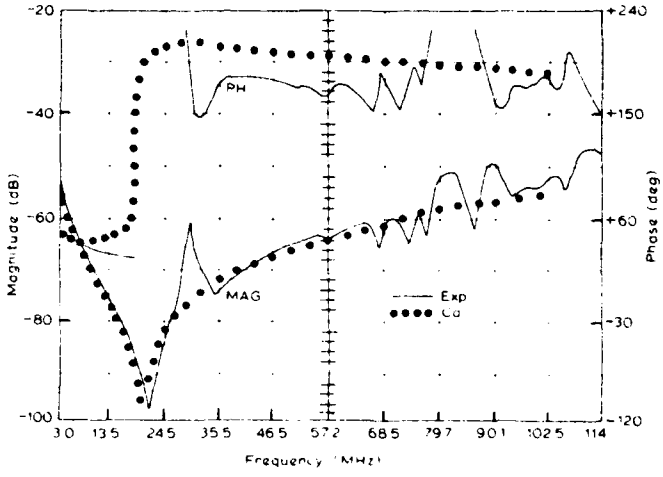

Figure 3.3 Amplitude and Phase Responses of JFET Amplifier after Model Parameter Adjustments (taken from [3.1])

Since this nonlinear interaction of the electromagnetic interference involves square-law detection of 1200 Hz in-band amplitude modulation from the interferer, it is necessary that the amplifier be terminated in a high impedance at low frequencies when nonlinear responses are to be determined. Therefore, the broadband input impedance of test instrumentation and connecting cables must be included in any model hoping to adequately model the nonlinear response. The nonlinear audio responses are at millivolt levels at the amplifier output. This dictates the need for an audio spectrum analyzer with good selectivity and gain. The HP 3580A spectrum analyzer was employed in all of our measurements of audio outputs. The input impedance is nominally 1 megohm paralleled by 30 pF over the 5-Hz to 50-kHz frequency range. Outside this region, major redistributions of voltages within the amplifier are caused by the analyzer, particularly at frequencies above 100 MHz.

(4) Determine the Linear Response at the Nonlinearity

The purpose of developing a good linear circuit model is to permit accurate estimates of the response of the model at the location of the nonlinearity. When this is done, the nonlinear response can be accurately calculated. For the JFET amplifier, the dominant nonlinearity is the square-law term in the nonlinear dependence of drain current upon gate-source voltage. Therefore, we must be able to accurately estimate the equivalent of voltage V between nodes 6 and 7 of Figure 3.1. This voltage is interior to JFET Q1. There is no chance of measuring this voltage except indirectly by measuring the nonlinear response at the amplifier output.

(5) Model the PC Etch and Test Fixture

The linear model illustrated in Figure 3.1 accounts for the discrete components in the amplifier and attempts to account for parasitic elements in these components. Inspection of the preamplifier PC board layout and test fixture (Figures 2.9 and 2.10)

shows the distributed nature of the actual circuit and test fixture. Elementary calculations show that the distributed capacitance and inductance of the etch is comparable to and can easily exceed the parasitic elements assigned to components. Excitation of the amplifier by the case ground is entirely through these "parasitic" etch components.

(6) Model the Inductor L1 at Radio Frequencies

The model of inductor L1 employed in Figure 3.1 is a low-frequency audio model that has such high impedances above 100 kHz that it might as well be omitted entirely. Measurements on the inductor indicate that a completely different three-terminal network model that cannot be represented by lumped R, L, and C's is necessary. For case excitation, the shield around the inductor serves to inject signals directly into the circuit by parasitic-capacitive coupling.

3.3 Low- and Medium-Frequency Model - Normal Excitation

Prior to developing a detailed model for the 1 - 500 MHz spectral region, it is relevant to present the results obtained for normal input excitation for the JFET amplifier in the 100 Hz to 1000 kHz region. In this region, the voltage gain is essentially controlled entirely by the basic components present in the schematic diagram of the amplifier with only minor dependence upon parasitic elements. Figure 3.4 shows such a linear equivalent circuit model. Parameter values for this model are listed in Table 3-1. There are 13 independent node voltages, all of which are with respect to the common node at the bottom of the figure. There are also 27 branches identified in the model. The model is excited by generator VG = 1 volt. Generator source impedance is RG = 50 ohms. The signal output, V_{11}, is at node 11 across the high impedance input of an oscilloscope that was used to observe the output experimentally. The scope model is 1 megohm paralleled by 20 pF capacitance. The linear voltage gain of the amplifier is defined as $H_1(f) \triangleq V_{11}/VG$.

Parasitic elements CR2, LC5, and RC5 as well as Q1 components CGS, RS, RD, and C13 could have been omitted without significantly changing the results. It is important to include CR3 and C11 in the model since they form a capacitive voltage

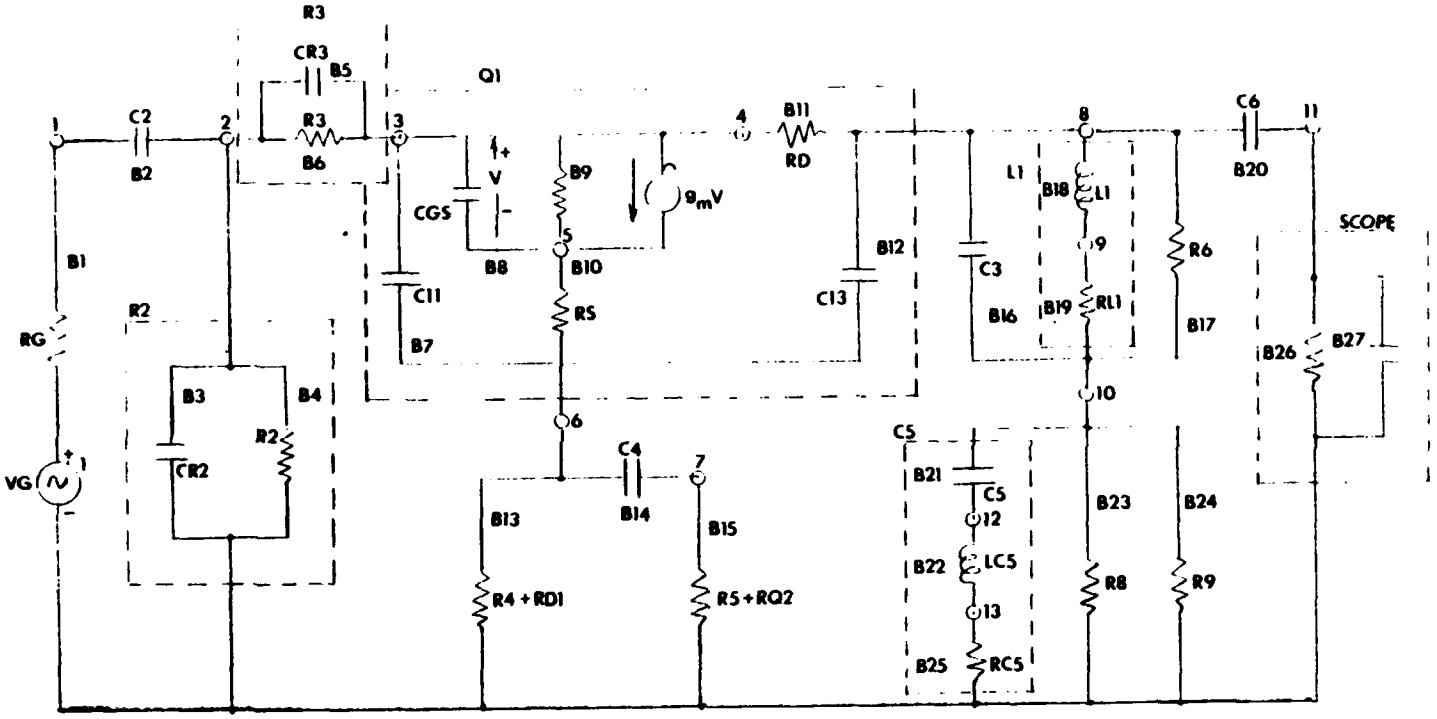

Figure 3.4 Low- and Medium-Frequency Equivalent Circuit Model of JFET Amplifier (Normal Excitation)

TABLE 3-1

I/CAP LISTING OF COMPONENTS FOR LOW-FREQUENCY MODEL

```
2:       LS
3:       AC
4: B1    N(1,0),R=50.0,E=1.0/180.0; RG,VG,NORMAL EXCITATION
5: B2    N(1,2),C=8.2E-11; C2
6: B3    N(2,0),C=0.4E-12; CR2
7: B4    N(2,0),R=1.0E6; R2
8: B5    N(2,3),C=0.23E-12; CR3
9: B6    N(2,3),R=3.3E4; R3
10: B7   N(3,6),C=0.9E-12; C11
11: B8   N(3,5),C=1.55E-12; CGS
12: B9   N(4,5),R=1.0E6; FICTIONAL
13: B10  N(5,6),R=37.0; RS
14: B11  N(4,8),R=37.0; RD
15: B12  N(8,6),C=0.38E-12; C13
16: B13  N(6,0),R=33.25E3; R4+RD1
17: B14  N(6,7),C=1.0E-6; C4
18: B15  N(7,0),R=474.0; R5+RQ2
19: B16  N(8,10),C=2.2E-9; C3
20: B17  N(8,10),R=1.5E5; R6
21: B18  N(8,9),L=7.36; TOROID(LF MODEL)
22: B19  N(9,10),R=640.0; TOROID(LF MODEL)
23: B20  N(8,11),C=1.03E-7; C6
24: B21  N(10,12),C=2.2E-5; C5,
25: B22  N(12,13),L=11.9E-8; LC5
26: B23  N(10,0),R=3.9E3; R8
27: B24  N(10,0),R=1.5E3; R9
28: B25  N(13,0),R=3.8,RC5
29: B26  N(11,0),R=1.0E6; SCOPE(RESISTIVE)
30: B27  N(11,0),C=20.0E-12; SCOPE(CAPAC.)
31: T1   B(8,9),GM=4.27E-4
```

divider having considerable impact upon the gate-to-source voltage V (nodes 3 - 5). The remaining circuit values are either the same as previously used by Whalen and Paludi, or have been adjusted to bring the model prediction into close agreement with the actual measurements. Note that the specific amplifier used to obtain experimental data was not the same physical amplifier used by Whalen and Paludi although it was of the same design and physical construction. The value of C3 in the amplifier was 2200 pF. R6 was 150 kilohms. Inductor L1 was determined to be 7.36 henries in order for the low-frequency resonance to be at 1240 Hz as measured. The Q of L1 was calculated to be about 72 in order for the bandwidth to be close to measured data. Note that the model for L1 is only of value near or below the resonant frequency.

An analysis of the circuit model to obtain voltage gain H_1 was performed using an Interactive Electronic Circuit Analysis Program (I/CAP) which was available through a remote terminal on a commercial timesharing computer service. The results of this analysis are shown in Figure 3.5 together with the measured gain of the experimental amplifier in the test jig. The very close agreement over four decades of frequency gives one confidence that the basic circuit components have been accurately modeled and that extension to wider bandwidths will require the addition of further parasitic elements or an entirely new mechanism without the need to modify the parameters of those elements already present. Inductor L1, however, will require an entirely new model.

3.4 Discussion of Circuit Model Parameters

The reader will recognize that we have not discussed how component values were obtained for the model other than to note that we either used values previously employed by Whalen and Paludi or modified their values where necessary to bring the prediction into agreement with the measurement. First, for the components that are in the schematic, we employ the nominal value of the component. As for parasitics, the use of manufacturers' data for the component is recommended. Components, when the risk of destroying a component is acceptable, can be removed from the amplifier and measurements attempted. Whalen and Paludi discuss their approach to this problem. Suffice it to say that we have not devoted much effort to this aspect of modeling for several reasons. One reason is that experience has shown that these methods only give crude results. If the

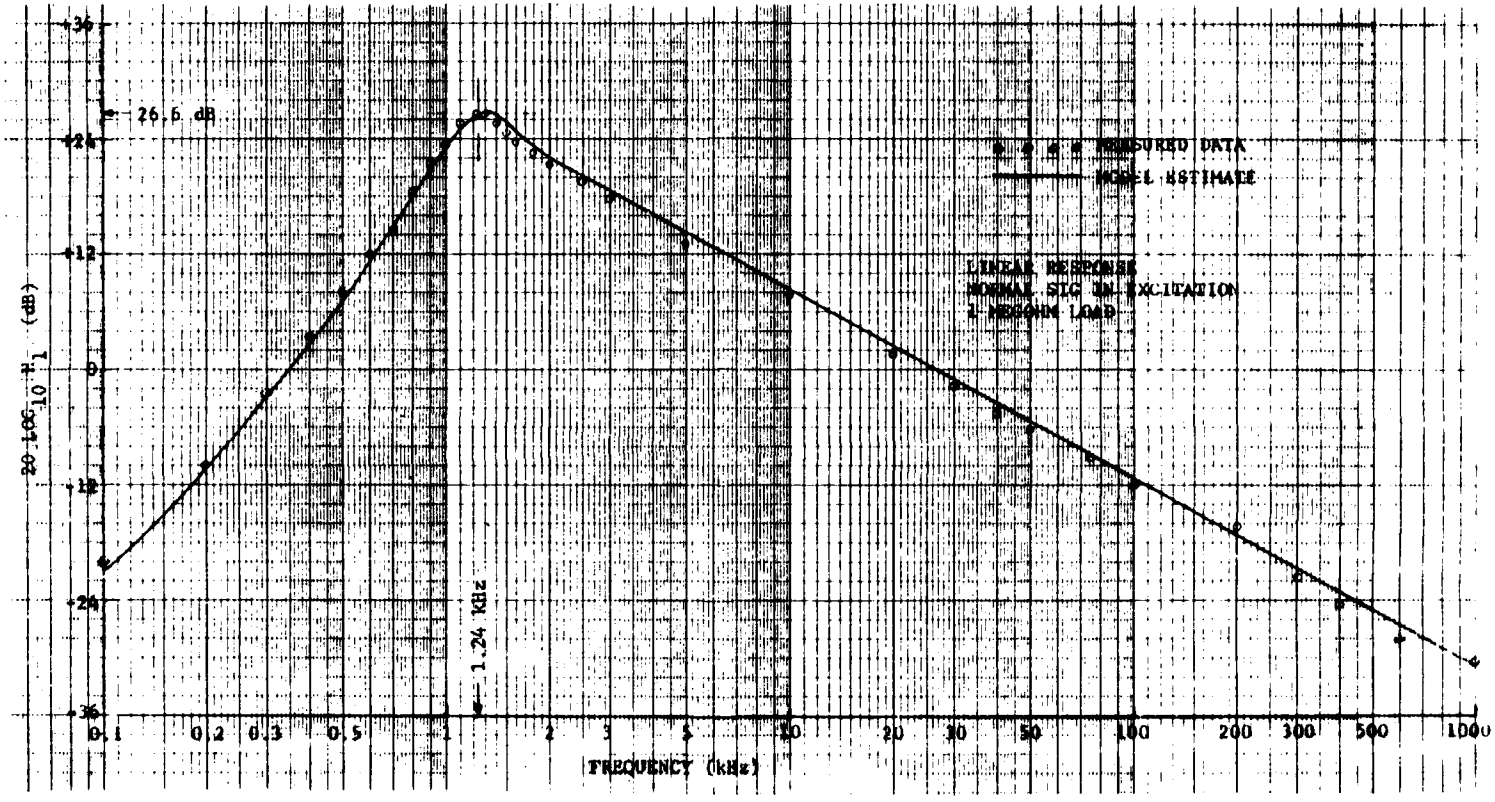

Figure 3.5 Comparison of Predicted and Measured Voltage Gain (Magnitude) of the Low- and Medium-Frequency Model

parasitic component has a substantial impact upon the circuit performance such as is the case when its value controls a zero or pole of transmission and, provided the interaction is with a nominal component from the schematic, it is usually necessary to adjust the component value on the basis of the pole or zero of transmission in order to retain adequate accuracy. Even this approach gets into difficulty when we encounter the situation where a zero or pole is controlled by the interaction of two parasitic elements as can happen at higher VHF and UHF regions. We have also noted that sometimes the experience of adjusting parasitic elements to bring predictions into agreement with measurements results in the conclusion that an unaccounted-for physical mechanism is present in the circuit that has not been included in the model. Major changes to the model configuration are necessary rather than more accurate values for the existing model. Finally, the whole aspect of parasitic element values, when the component is in situo in a PC board with obvious PC etch capacitive and inductive values comparable to or exceeding the component parasitic element, raises serious questions about the utility of modeling component parasitics but ignoring the PC etch. As we have noted for the amplifier under examination, excitation of the case ground excites the PC etch.

The model of the JFET is also drawn from Whelan and Paludi. The value of g_m is from 1-kHz measurements but is also confirmed by the results in Figure 3.5. Q1 capacitive parameters are from 1-MHz measurements that were subsequently improved upon by s-parameter measurements in the 200 - 400 MHz region. We have found it necessary to adjust C11 to bring the model prediction into agreement with our measurements. The remaining parameters of the model do not seem to have much impact upon performance throughout the 1 - 500 MHz region. Other external mechanisms dominate. It is interesting to note that insofar as the linear response of the amplifier is concerned above 10 MHz, it makes little difference whether the amplifier has dc power applied or not! The coupling to the SIG OUT terminal for both SIG IN and CASE GROUND excitation is dominated by the capacitive elements in the circuit rather than by the active current source in the JFET.

3.5 Modeling the Inductor L1

Modeling inductor L1 presented some difficulties. First, it was recognized that the audio low-frequency model would not be satisfactory. This is particularly true when the CASE GROUND

terminal is excited. The inductor with its shielding case forms a three-terminal passive network, as shown in Figure 3.6(a). Therefore, a possible equivalent circuit model for the inductor is the pi-network such as shown in Figure 3.6(b). The most convenient experimental method of obtaining broadband data to characterize the inductor over the 1 - 500 MHz region is to insert the inductor in a simple series test jig with the case serving as a common ground and measure the s-parameters with a network analyzer for the resulting structure. Table 3-2 lists the results of such a measurement on the inductor from the test amplifier. The forward transmission loss with 50-ohm terminations on the test jig is plotted in Figure 3.7. Figure 3.8 shows the input admittance (obtained from S11) as a function of frequency on a Smith chart for the inductor with a 50-ohm load at the output. We note the following characteristics of the inductor from this data. The input admittance is lossy and inductive over the range 1 - 150 MHz. Between about 150 and 210 MHz, the admittance becomes capacitive with a return to inductive above 210 MHz. Examination of the data in Table 3-2 indicates that the inductor is not quite symmetrical ($S_{11} \neq S_{22}$). The forward and reverse transmission losses should be the same and are nearly so since the network is passive and, therefore, reciprocal ($S_{12} = S_{21}$). The null near 210 MHz in the forward transmission might have been caused by parallel-resonance between the input and output terminals, but the input admittance series-like resonance at 210 MHz indicates that the cause of the large loss in transmission near 210 MHz is shunt-loading caused by a series resonance involving capacitance to the inductor case. These clues to the inductor characteristic strongly suggest that a rough model of inductor L1 should have a series L and C in both the Y_a and Y_b arms of the pi-network. The LC product should be adjusted to resonate near 200 MHz. Examination of input admittances off the resonances suggests that C is of the order of 20 pF.

It is convenient from a computer-aided circuit analysis point-of-view to have the inductor modeled with fixed-value lumped R, L, and C elements. This is not possible, however, even for a rough model of the Y_c branch in the pi-network. The reason is that the ferrite magnetic-core losses are frequency-dependent and the impedance of the inductor assumes an entirely different character. An approximation that is simple to use for a rough model is given by

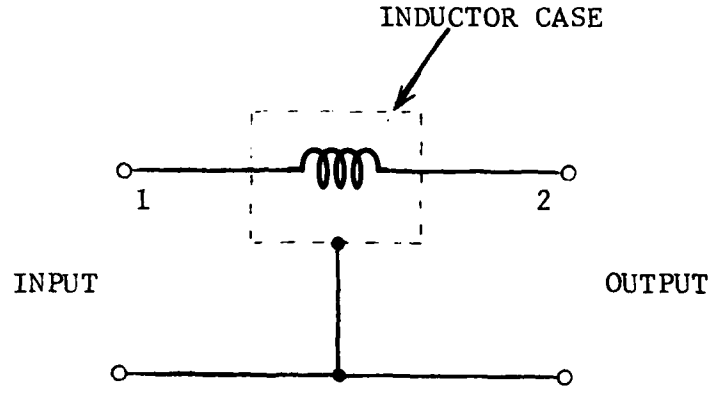

(a) Three-Terminal Inductor L1

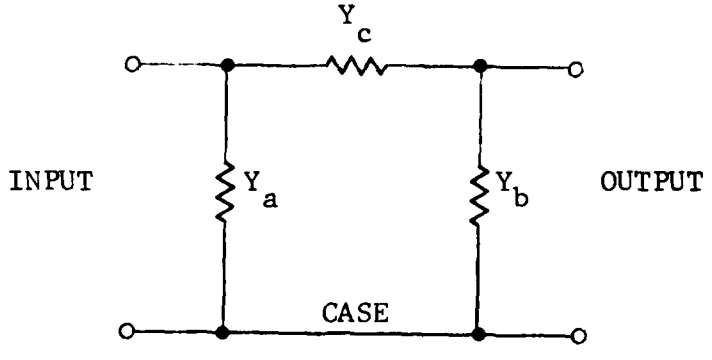

(b) Pi-Network Equivalent Circuit

Figure 3.6 Inductor L1 as a Three-Terminal Network

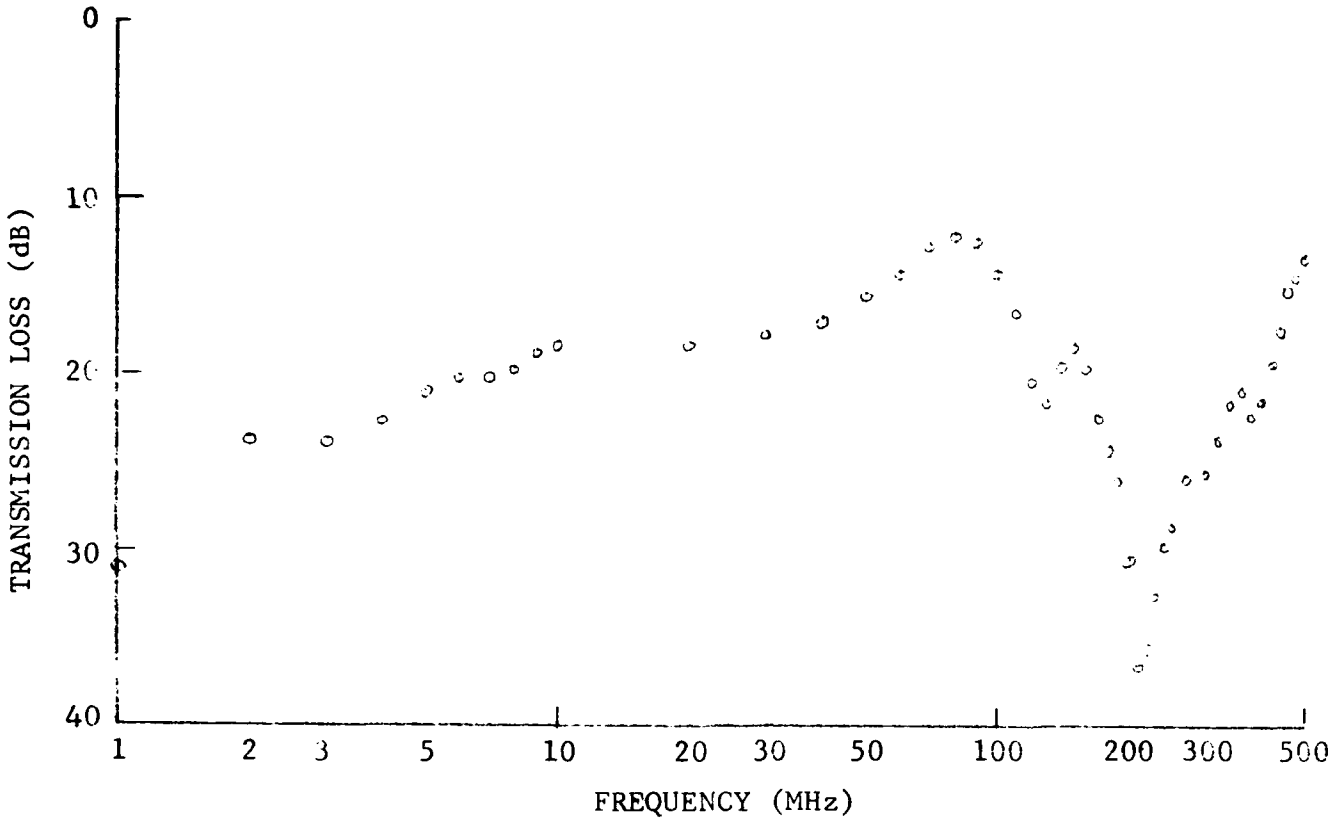

Figure 3.7 Forward Transmission Loss of Inductor L1 in Test Jig

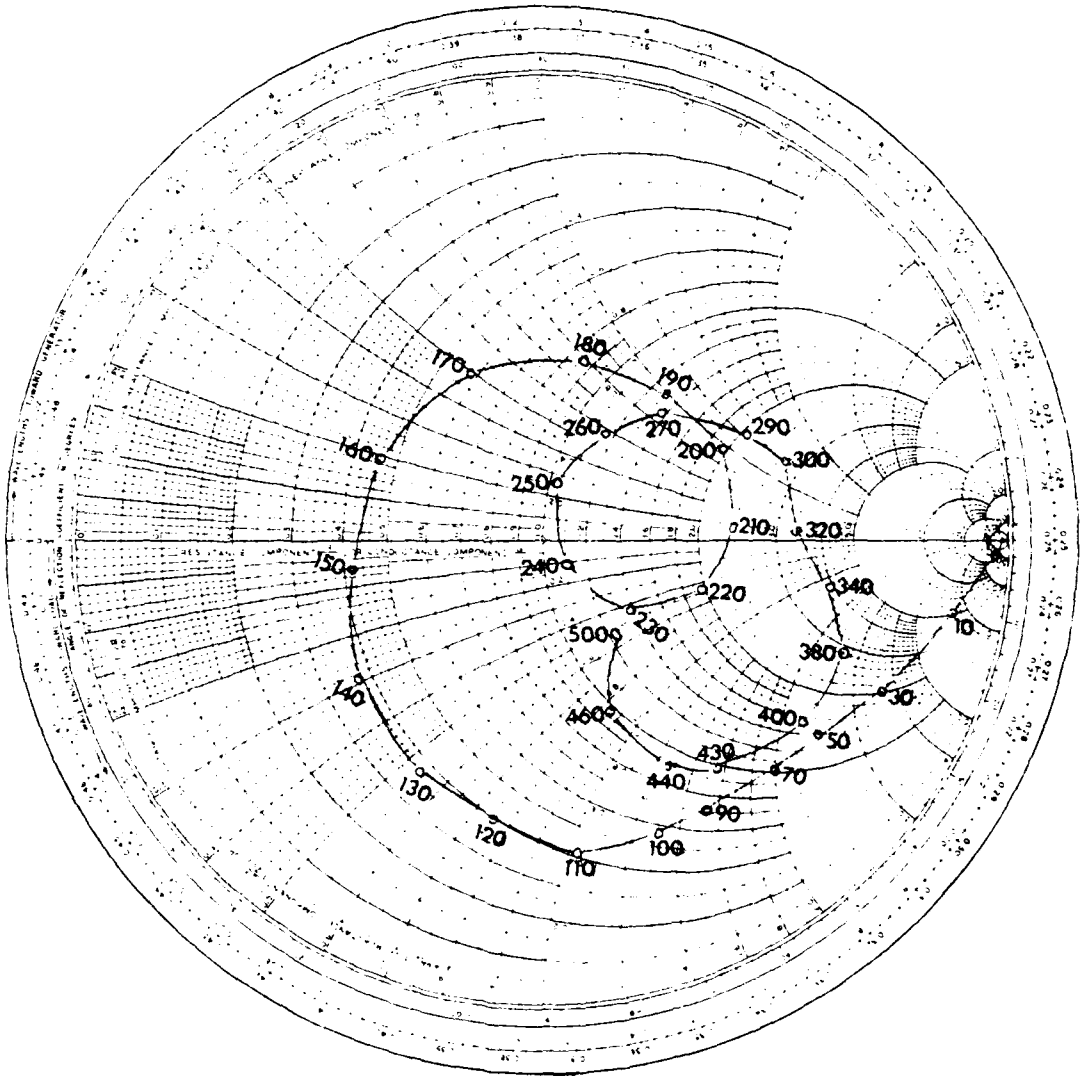

Figure 3.8 Input Admittance of Inductor L1 in Test Jig

TABLE 3-2

S-PARAMETERS OF INDUCTOR L1 IN TEST JIG

FREQUENCY MHZ	RETURN LOSS INPUT (S11) DB	ANG	TRANS. LOSS FORWARD (S21) DB	ANG	TRANS. LOSS REVERSE (S12) DB	ANG	RETURN LOSS OUTPUT (S22) DB	ANG
1.000	0.3	-1.8	31.06	34.0	31.00	33.9	0.2	-2.5
2.000	0.8	-3.7	23.75	13.8	23.75	13.8	0.5	-4.0
3.000	0.8	-2.9	24.13	25.7	24.11	25.7	0.5	-6.7
4.000	0.7	-4.9	22.67	32.7	22.74	32.7	0.6	-8.8
5.000	0.8	-6.4	21.19	30.4	21.14	30.4	0.7	-10.6
6.000	0.9	-7.1	20.38	25.9	20.43	25.9	0.9	-12.0
7.000	1.0	-7.3	20.36	24.7	20.40	24.7	1.0	-13.5
8.000	1.0	-8.1	19.83	26.5	19.86	26.5	1.1	-15.4
9.000	1.0	-9.2	18.90	24.6	18.92	24.6	1.4	-17.1
10.000	1.1	-9.9	18.37	19.6	18.38	19.6	1.6	-18.0
20.000	1.3	-17.3	18.56	9.4	18.55	9.5	2.7	-19.7
30.000	2.0	-24.3	17.81	9.5	17.80	9.5	2.5	-26.4
40.000	2.4	-30.4	16.69	9.3	16.69	9.2	2.4	-35.9
50.000	2.9	-35.6	15.52	4.7	15.53	4.6	2.4	-48.1
60.000	3.3	-38.9	14.37	-3.0	14.39	-3.0	2.5	-65.9
70.000	3.1	-45.8	12.83	-11.0	12.84	-11.1	3.5	-89.5
80.000	3.4	-51.3	12.22	-29.1	12.24	-29.1	5.8	-123.1
90.000	3.4	-59.2	12.52	-49.1	12.55	-49.1	9.3	-175.7
100.000	3.3	-69.4	14.37	-66.6	14.39	-66.5	12.6	102.9
110.000	3.4	-84.4	16.61	-77.9	16.63	-77.8	9.5	44.8
120.000	4.4	-100.6	20.54	-81.0	20.56	-80.8	7.2	7.4
130.000	5.0	-118.2	21.77	-60.6	21.79	-60.6	6.8	-20.8
140.000	6.2	-142.7	19.81	-55.7	19.74	-55.8	7.4	-48.0
150.000	7.8	-171.1	18.56	-72.3	18.58	-72.2	10.7	-76.7
160.000	8.4	154.6	19.87	-91.3	19.88	-91.1	17.9	-75.7
170.000	8.3	113.0	22.55	-103.2	22.58	-103.1	16.2	-45.7
180.000	8.0	77.0	24.31	-108.6	24.34	-108.8	14.6	-79.5
190.000	7.7	49.5	26.19	-128.9	26.22	-129.0	18.1	-146.3
200.000	7.3	26.9	30.65	-162.6	30.67	-162.9	13.6	114.3

TABLE 3-2 (Continued)

FREQUENCY	RETURN LOSS INPUT (S11)		TRANS. LOSS FORWARD (S21)		TRANS. LOSS REVERSE (S12)		RETURN LOSS OUTPUT (S22)	
MHZ	DB	ANG	DB	ANG	DB	ANG	DB	ANG
210.000	7.6	4.4	36.90	128.4	36.82	128.6	20.7	59.5
220.000	9.1	-17.4	35.63	63.3	35.54	63.5	22.2	113.4
230.000	12.8	-38.2	32.61	46.5	32.51	46.6	11.9	108.2
240.000	23.5	-44.5	29.97	37.3	29.97	37.2	7.7	82.5
250.000	18.2	75.5	28.67	31.6	28.67	31.7	5.8	60.6
260.000	11.3	61.9	27.09	29.9	27.09	30.0	5.0	43.0
270.000	8.5	48.0	25.89	24.1	25.91	24.4	4.9	28.6
280.000	7.1	36.9	25.34	18.7	25.36	19.0	5.3	17.6
290.000	6.1	27.7	25.28	11.4	25.29	11.1	5.9	12.0
300.000	5.3	18.4	25.66	19.2	25.69	19.4	5.9	11.1
310.000	5.0	8.2	24.94	22.9	24.88	23.1	5.5	5.8
320.000	5.4	1.8	23.71	24.9	23.64	24.9	5.5	-0.8
330.000	5.6	-0.1	22.47	22.4	22.50	22.4	5.7	-7.7
340.000	5.2	-0.9	21.63	17.9	21.65	17.9	6.6	-14.0
350.000	4.6	-3.8	21.13	12.6	21.14	12.5	8.1	-14.2
360.000	4.1	-8.6	21.01	7.0	21.01	7.0	8.8	-4.4
370.000	3.6	-13.9	21.58	3.0	21.58	2.9	7.8	3.7
380.000	3.3	-20.5	22.31	4.9	22.32	5.1	6.4	2.2
390.000	3.2	-27.6	22.28	11.2	22.19	11.3	5.7	-2.9
400.000	3.4	-34.4	21.48	16.1	21.50	16.2	5.4	-7.3
410.000	3.6	-40.2	20.56	18.8	20.48	18.6	5.2	-11.7
420.000	3.8	-46.2	19.45	19.9	19.39	19.7	5.3	-16.8
430.000	4.3	-53.5	18.31	18.5	18.26	18.4	5.8	-20.3
440.000	5.1	-61.1	17.29	16.2	17.25	16.3	6.5	-18.7
450.000	6.5	-67.2	16.15	13.1	16.22	13.0	6.2	-13.2
460.000	8.4	-68.4	15.21	7.2	15.27	7.3	5.2	-12.0
470.000	9.9	-62.7	14.66	0.9	14.70	0.8	4.4	-15.6
480.000	10.4	-56.0	14.36	-4.0	14.39	-3.9	4.0	-21.0
490.000	10.8	-53.6	13.99	-7.2	13.90	-7.2	3.9	-25.9
500.000	11.9	-51.2	13.25	-11.3	13.25	-11.2	4.2	-28.7

$$Z_c = \frac{1}{Y_c} \cong \frac{(1+j)}{\sqrt{\omega}} \, k \quad \text{ohms}$$

with k to be adjusted to reasonably fit the insertion loss data in the region where the series resonance is not dominant.

Figure 3.9 shows a comparison between the transmission loss of the pi-network model shown on the figure and the measured loss for $k = 5.29 \times 10^6$. The model shown is the final model after adjustment to the shunt L and C elements to provide the best fit to measured data in the amplifier model.

The reader will recognize that not all of the experimental measurement information available in the measured s-parameters has been utilized in devising the rough model of inductor L1. Experience with the model shows that the amplifier response is not very sensitive to the model used for the Y_c branch of the pi-network. This is because the capacitance C3 is directly in parallel with Y_c. C3 is large and the impedance of the model for C3, including its series inductance, is such that throughout the 1 - 500 MHz region the impedance does not exceed a few ohms at most. The amplifier model with case excitation is more sensitive to the Y_a and Y_b branches of the pi-network. Element values in these branches interact with the PC etch to cause a significant shift of the effective null frequency away from 210 MHz to a much lower frequency. One of our recommendations for improvement of the inductor model is to utilize the complete s-parameter data. If this is done, a value for Y_a, Y_b, and Y_c for each frequency at which the s-parameters were measured becomes available. I/CAP, the computer-aided circuit analysis program available to us does not have the capability of incorporating such data in the model other than by a new equivalent R, L, or C at each frequency. If one wishes to proceed in this manner, it is possible to express the A, B, C, and D matrix parameters of the two-port model of the inductor in terms of the s-parameters. The admittance matrix parameters follow directly from ABCD elements. The final step is determination of Y_a, Y_b, and Y_c for the pi-network from the admittance matrix.

3.6 Modeling the PC Etch and the Space between the Case Ground and External Ground

Our first modeling efforts for the printed-circuit board involved incorporating capacitance between the etch and the case

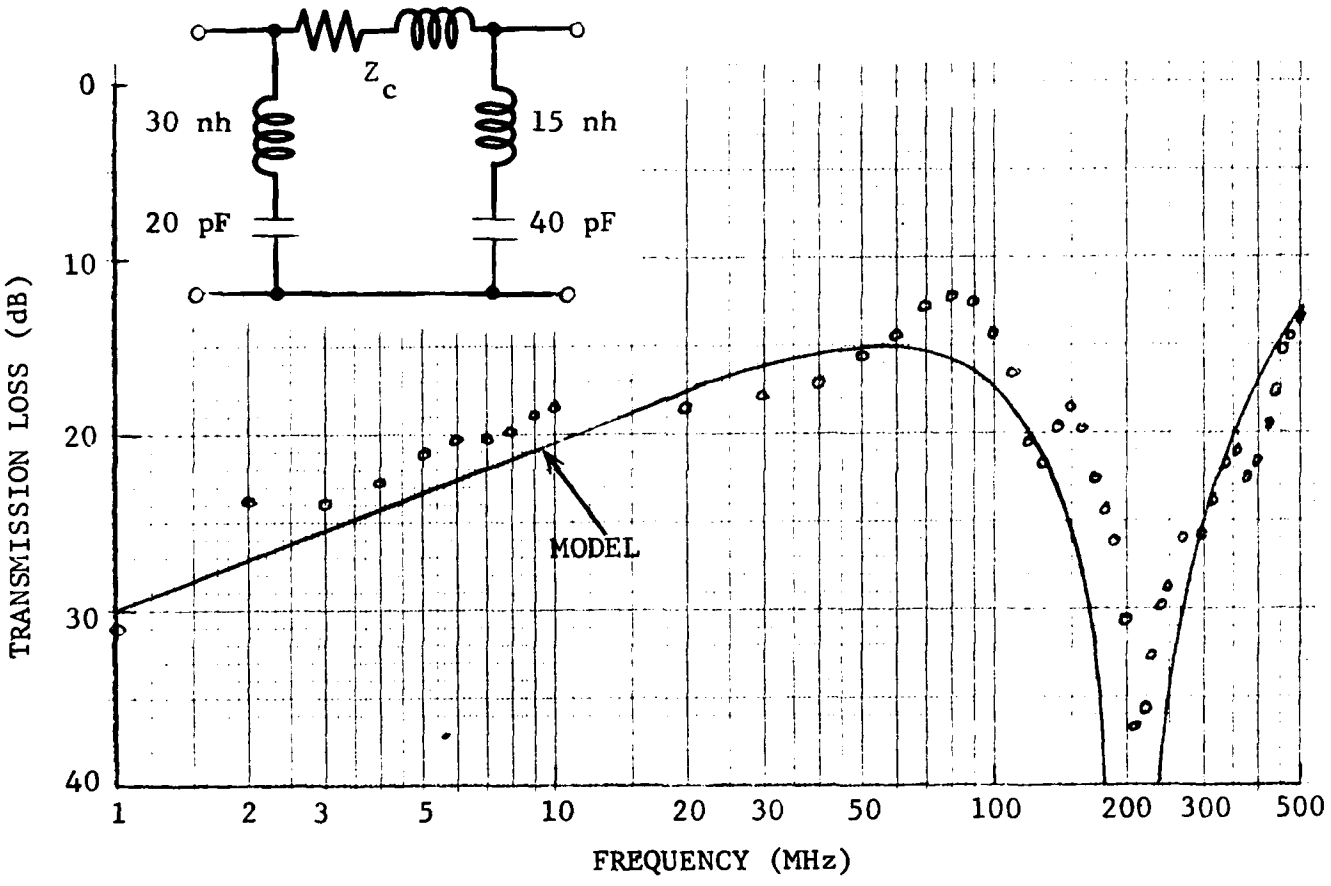

Figure 3.9 Comparison of Inductor L1 Model with Experimental Measurements [$Z_c = 5.29 \times 10^6 (1+j)/\sqrt{\omega}$]

ground. This model is satisfactory for those portions of the etch that are short, say, of no greater than approximately an inch in length. It proved inadequate for several of the larger etches (see Figure 2.9).

A better model for the PC etch is a transmission line. The characteristic impedance and delay per unit length of the line are determined by the capacitance and inductance per unit length of the etch in proximity with the case ground. These parameters are determined by the physical dimensions and dielectric properties of the transmission line cross section. Total delay is dependent upon the length of the transmission line. For a transmission line model to be of practical value when we use I/CAP, it is necessary that we employ a lumped parameter model rather than a distributed circuit model. A symmetrical-T meets this requirement, but it must be recognized that care must be exercised not to attempt to use a single symmetrical-T section over too large a bandwidth. A rule-of-thumb is to limit the phase delay to less than 90 degrees. Figure 3.10 summarizes the pertinent relationships for a symmetrical-T model of a transmission line. An appreciation of the numerical values involved in modeling a length of PC etch is presented by the following example. For an epoxy-glass dielectric constant $k = 4$, we expect 2 ns delay/foot or about 0.5 ns delay in a 3-inch length. The etch transmission line characteristic impedance is about 220 ohms. It follows that $L = 110$ nh or about 37 nh/inch and $C = 2.3$ pF or about 0.76 pF/inch. Using the 90^{o} phase shift ($\lambda/4$ wavelength) criteria, the symmetrical-T section for a 3-inch section of PC etch should not be used above $f = 1/4\tau = 500$ MHz. An even more conservative model would limit the phase delay to 45^{o} maximum. The choice of which section of PC etch to model with symmetrical-T sections requires close examination of the circuit board layout. It is desirable to limit the application of this model to those sections of etch that are likely to introduce substantial delay. Experience with the model shows that it must be employed to adequately account for some of the significant effects above 200 MHz.

A delay line model consisting of two cascaded symmetrical-T sections is necessary to model the cavity between the case ground and the external ground plane of the test box (see Figure 2.10). Two sections are necessary because the delay exceeds 0.5 ns. The characteristic impedance of the cavity to a TEM mode wave is about 21 ohms. The reader will recall, from the discussion in Section 2, that suppression of the

(a) TRANSMISSION LINE

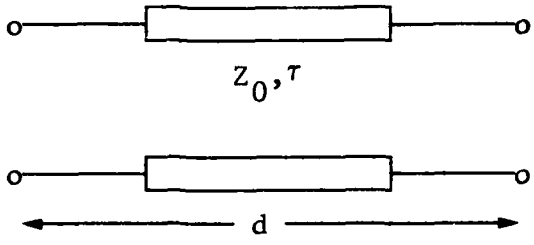

ℓ = INDUCTANCE/UNIT LENGTH
c = CAPACITANCE/UNIT LENGTH

$$Z_0 = \sqrt{\frac{\ell}{c}} \quad ; \quad \tau = d\sqrt{\ell c}$$

(b) SYMMETRICAL-T MODEL OF TRANSMISSION LINE

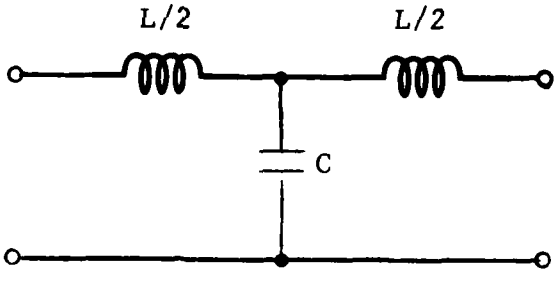

$$L = \ell d = Z_0 \tau \quad ; \quad C = cd = \frac{\tau}{Z_0}$$

$$Z_0 = \sqrt{\frac{L}{C}} \quad ; \quad \tau = \sqrt{LC}$$

FOR $\theta < 90^\circ$, $\omega < \frac{\pi}{2} \frac{1}{\sqrt{LC}}$ OR $f < \frac{1}{4\tau}$

Figure 3.10 Symmetrical-T Model of Transmission Line

external cable excitation by strapping the signal ground to the external ground plane did not suppress excitation of the cavity between the case ground and the external ground.

3.7 Linear Model of the Amplifier and Test Circuit

When the more complete linear models for PC etch, inductor L1, JFET Q1, and other passive components are combined in one equivalent circuit to model the test amplifier in the test circuit configuration, we have a fairly complete linear equivalent circuit structure that has been found to be reasonably valid throughout the 1 - 500 MHz region. Figure 3.11 presents such a model. Table 3-3 provides an I/CAP listing of the final circuit parameter values by branch and node pair.

Excitation of the equivalent circuit is by generator VG with resistive source impedance RG. The excitation can be applied either at the SIG IN (nodes 1 - 0) or at CASE GND (nodes 2 - 0). The load impedance Z_L at the output is always between SIG OUT and SIG OUT GND (nodes 21 - 24). The listing in Table 3-3 indicates that $Z_L = 10^6$ ohms, but the value employed depends upon the situation being evaluated. We shall explicitly state what the load is when we discuss the results of model prediction. Linear measurements typically used 50-ohm loads. When the model is used to predict nonlinear response, the load impedance must be the input impedance of the audio spectrum analyzer at the carrier radio frequency exciting the network.

Models for the circuit components from the amplifier schematic (Figure 2.3) are enclosed within dashed-line boxes and labeled with their associated component label. Specific values for the parameters of each model can be found in Table 3-3. Branches B39 - B47 model the capacitive coupling between the PC etch and case ground. Generally, these branches are associated with short lengths or noncritical lengths of PC etch. The reader will note that branch B41 provides direct coupling to the JFET (Q1) input (node 5) from excitation of the case ground (node 2). This coupling and, to a lesser degree, branch B40 are the primary means of exciting the nonlinearity in Q1 when the amplifier case is excited. Although the capacitance in branch B41 is only 0.15 pF, a substantial portion of the case ground excitation appears across nodes 5 - 6 because the input capacitances in Q1 are, themselves, quite small (branch B9: 0.9 pF; branch B10: 1.55 pF). Experience with the model proved it necessary to introduce transmission models for the PC etch

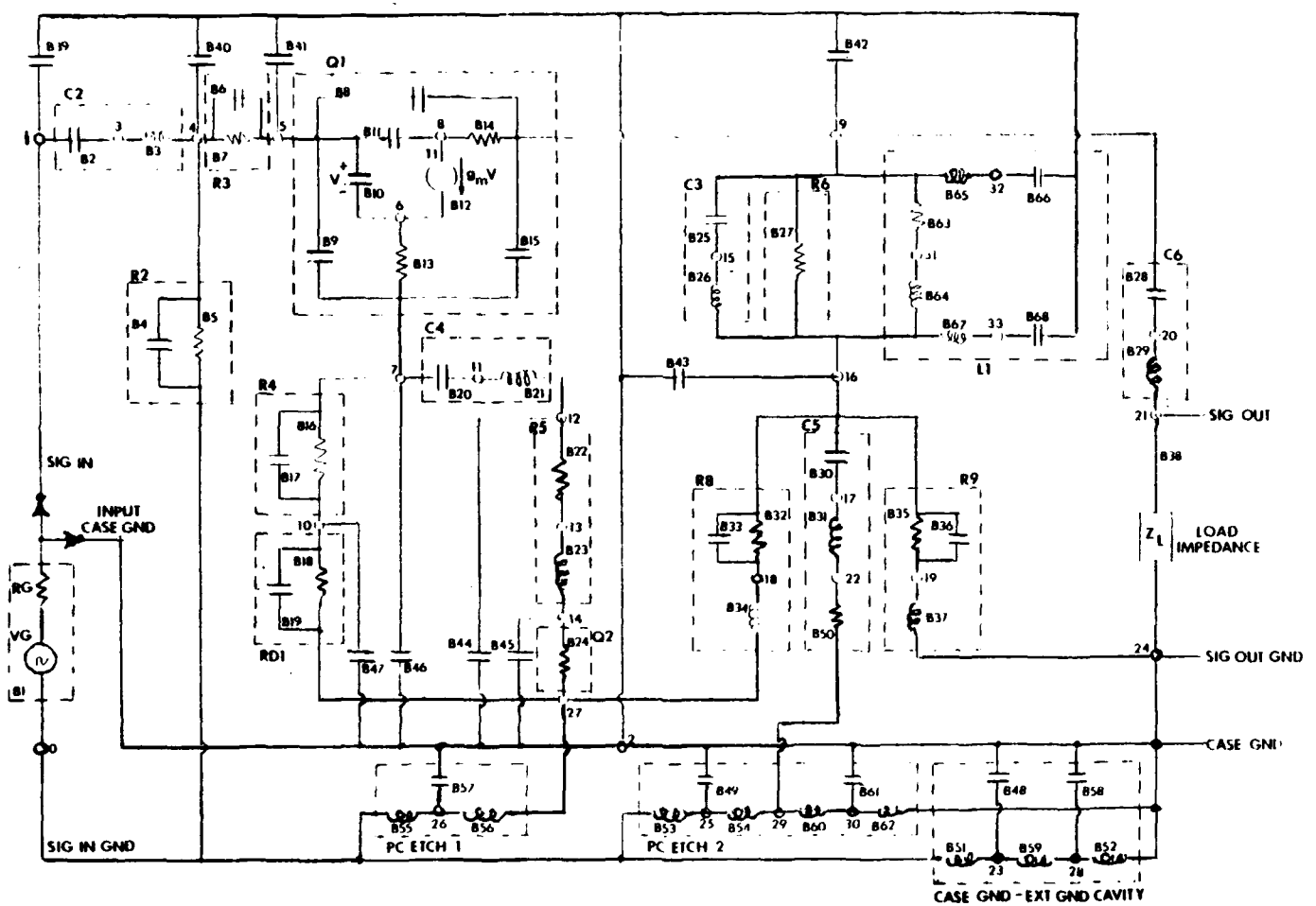

Figure 3.11 Linear Circuit Model of JFET Amplifier and Test Box for Frequencies less than 500 MHz

TABLE 3-3

I/CAP LISTING OF EQUIVALENT CIRCUIT PARAMETERS

```
4: B1    N(2,0),R=50.0,E=1.0/180.0; RG,VG,CASE EXCITATION
5: B2    N(1,3),C=8.2E-11; C2
6: B3    N(3,4),L=1.0E-8; LG2
7: B4    N(4,0),C=0.4E-12; CR2
8: B5    N(4,0),R=1.0E6; R2
9: B6    N(4,5),C=0.23E-12; CR3
10: B7   N(4,5),R=3.3E4; R3
11: B8   N(5,9),C=1.0E-14; C12
12: B9   N(5,7),C=0.9E-12; C11
13: B10  N(5,6),C=1.55E-12; CGS
14: B11  N(5,8),C=0.09E-12; CGD
15: B12  N(8,6),R=1.0E6; FICTIONAL
16: B13  N(6,7),R=37.0; RS
17: B14  N(8,9),R=37.0; RD
18: B15  N(7,9),C=0.38E-12; C13
19: B16  N(7,10),R=3.3E4; R4
20: B17  N(7,10),C=0.4E-12; CR4
21: B18  N(10,27),R=250.0; RD1
22: B19  N(10,27),C=1.0E-11; CD1
23: B20  N(7,11),C=1.0E-6; C4
24: B21  N(11,12),L=1.0E-8; LG4
25: B22  N(12,13),R=200.0; R5
26: B23  N(13,14),L=2.5E-8; LR5
27: B24  N(14,27),R=274.0; RG2
28: B25  N(9,15),C=2.2E-9; C3
29: B26  N(15,16),L=1.0E-9; LG3
30: B27  N(9,16),R=1.5E5; R6
31: B28  N(9,20),C=1.03E-7; C6
32: B29  N(20,21),L=1.0E-8; LG6
33: B30  N(16,17),C=2.2E-5; C5
34: B31  N(17,22),L=42.0E-9; LG5
35: B32  N(16,18),R=3.9E3; R8
36: B33  N(16,18),C=0.4E-12; CR8
37: B34  N(18,27),L=2.5E-8; LR8
38: B35  N(16,19),R=1.5E3; R9
39: B36  N(16,19),C=0.4E-12; CR9
40: B37  N(19,24),L=2.5E-8; LR9
41: B38  N(21,24),R=1.0E6; OPEN CIRCUIT LOADING
42: B39  N(1,2),C=0.33E-12
43: B40  N(4,2),C=0.45E-12
44: B41  N(5,2),C=0.15E-12
45: B42  N(9,2),C=2.2E-12
46: B43  N(16,2),C=1.5E-12
47: B44  N(12,2),C=0.23E-12
48: B45  N(14,2),C=0.66E-12
49: B46  N(7,2),C=0.79E-12
50: B47  N(10,2),C=0.53E-12
51: B48  N(23,2),C=7.3E-12
52: B49  N(25,2),C=0.77E-12
53: B50  N(22,29),R=0.1
54: B51  N(0,23),L=2.3E-9
55: B52  N(28,24),L=2.3E-9
56: B53  N(0,25),L=18.6E-9
57: B54  N(25,29),L=18.6E-9
58: B55  N(0,26),L=55E-9
59: B56  N(26,27),L=55E-9
60: B57  N(26,2),C=2.2E-12
61: B58  N(28,2),C=7.3E-12
62: B59  N(23,28),L=3.2E-9
63: B60  N(29,30),L=18.6E-9
64: B61  N(30,2),C=0.77E-12
65: B62  N(30,24),L=18.6E-9
66: T1   B(10,12),GM=4.27E-4
     MODEL,N(9,2,16),P(2111.0,336.0U),TORMOP
MODEL EXPANSION:
67: C    ;ASSYMMETRIC TOROID
68: B63  N(9,31),R=2111.0
69: B64  N(31,16),L=336.0U
70: B65  N(9,32),L=15.0KUU
71: B66  N(32,2),C=40.0UU
72: B67  N(16,33),L=30.0KUU
73: B68  N(33,2),C=20.0UU
```

in two areas. These models are labeled PC Etch 1 and PC Etch 2 in Figure 3.11. PC Etch 1 models the delay in the PC board etch associated with the SIG GND from the SIG GND input at the ground strap (see Figure 2.9), and the rough average of the several circuit branches grounded to the etch in the vicinity of Q1 and Q2. Nonlinear responses to case ground inputs were significantly cut off above 200 MHz before the introduction of the PC Etch 1 model and the grouping of currents from RD1, Q2, and R8 before "grounding".

The components in the model labeled PC Etch 2 model the delay in the PC board etch and the "grounding" of C5 (see Figure 2.9) and the further delay in the connecting wire over the ground plane to the output (TB2 - 4). Finally, the components in the Case Ground-External Ground box model the coupling through the cavity between the case ground and external ground plane in the test box as previously described in Section 3.6.

3.8 Comparison of Calculated and Experimental Linear Responses

In this section we present the calculated insertion gain of the model shown in Figure 3.11 using the parameters from Table 3-3 and compare the results with measurements of insertion gain made on the amplifier test configuration. Figure 3.12 shows this information over the 1 - 500 MHz region when the excitation is applied to the case ground terminal and the output load is 50 ohms. Figure 3.13 presents the calculated and measured insertion gain when the SIG IN terminal is excited and the output load is 50 ohms. Note that above 1 MHz the insertion gain for case excitation exceeds that for normal signal input excitation.

For case excitation (Figure 3.12), the coupling to the 50-ohm output is dominated by excitation of the output through capacitive coupling through the PC etch and inductor L1 from case ground (node 2) to the output etch (node 9) and node 16. There is no significant contribution from Q1 active gain. The null near 11 MHz is caused by a resonance diverting the capacitively coupled current away from the 50-ohm output through a low impedance involving capacitance C3, the parasitic inductance LC5 of C5, and the inductance of the PC etch. The asymmetry of Y_a and Y_b branches in the model of inductor L1 plays a role in controlling the frequency of the "null" as well as the insertion gain above the null. For example (see Figure 3.11), greater

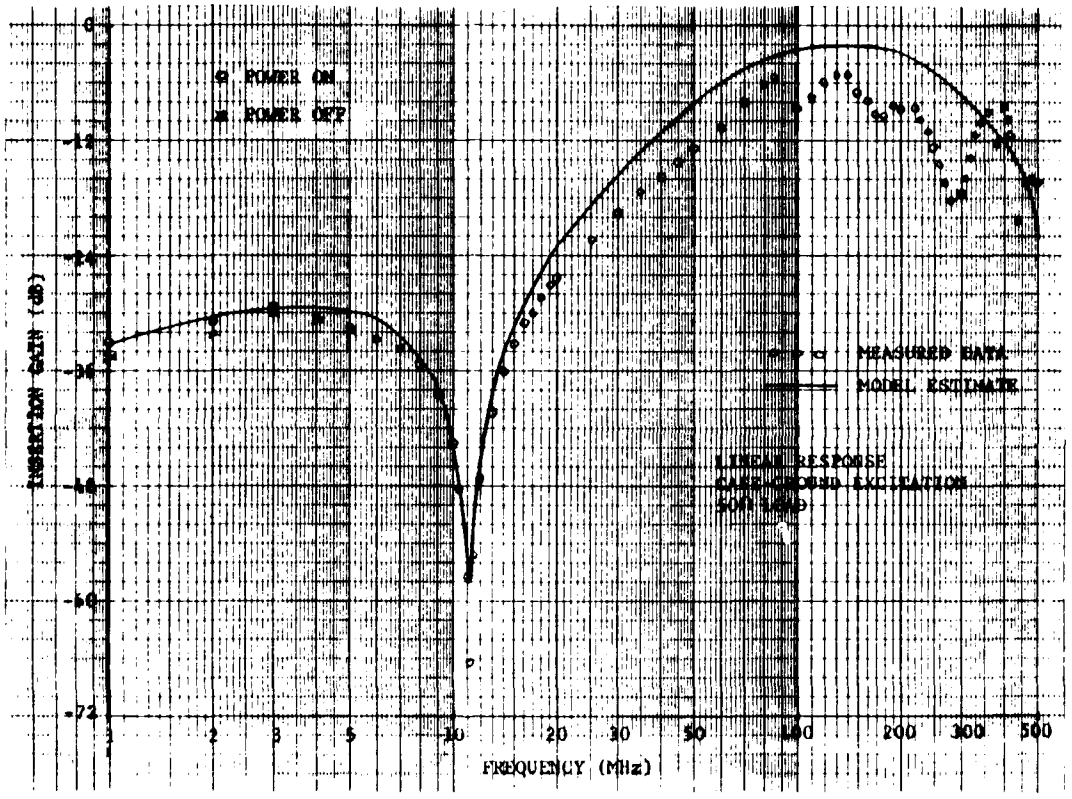

Figure 3.12 Case Ground Excitation Linear Response

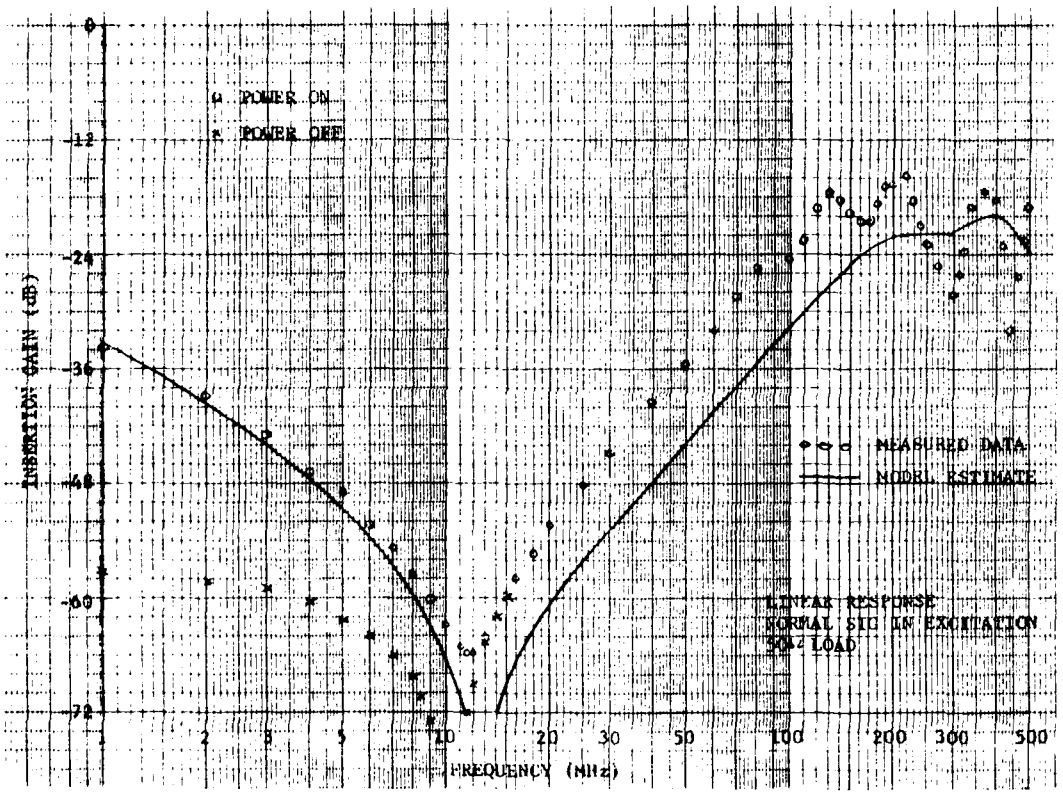

Figure 3.13 SIG IN Excitation Linear Response

coupling to node 16 through branches B43 and B68 causes greater current to flow through the inductance in branch B31. This shifts the resonance to a lower frequency and increases the insertion gain at frequencies above resonance.

For excitation at the SIG IN terminal (Figure 3.13), the coupling to the output at frequencies below the "null" near 12 MHz is dominated by the active gain of Q1, while above the resonance there is little contribution from the dependent current source in Q1. Coupling to the output is essentially entirely capacitive above the null. This resonant null is also caused by a diversion of current away from the 50-ohm output through a low impedance again involving capacitance C3, inductance LC5, and the inductance of the PC etch. The model of the inductor L1 does not have any significant impact upon this null. In the region between about 20 and 100 MHz, the slope of the insertion gain (Figure 3.13) is 12 dB per octave. This is as expected for a capacitvely-coupled source developing a voltage across the effective inductance of LC5 and the PC etch.

For case ground excitation, the model produces a gain approximately 5 dB greater than measured values over the 20 - 100 MHz range. The model also produces a gain approximately 8 dB lower than measured values over the same region for normal signal input excitation. Attempts were made to adjust the parameters of inductor Y_a and Y_b branches, and inductance LC5 to bring the model calculations into closer agreement with the measured data. The values employed represent the best compromise within the constraints of the model configuration. For example, increasing LC5 reduces the 8-dB deviation for signal input excitation but causes the case excitation response to increase beyond the 5 dB. It is suspected that a better model for the inductor and, particularly, its asymmetry might improve the model. Fuller utilization of the complete data for L1 (see Section 3.5) would be a starting point in such an effort.

Finally, the inductance of LC3 (branch B26) used in the calculation was 1 nh. Subsequent measurements on the self-resonant frequency of C3 indicated that a better value for LC3 is 7 nh. This change in parameter values would not alter the model prediction in a significant manner.

3.9 Further Comments

The reader will note that much of the complication in modeling the linear response of the amplifier involves the model of the components and PC etch in the output of the amplifier. If our main interest is in the nonlinear response of the model and our development of the linear model is for the specific purpose of enabling a calculation of the nonlinear response, our effort should concentrate upon the linear response at the site of the nonlinearity rather than the response at a 50-ohm load at the output. The nonlinearity operative in the amplifier is the dependence of the current source in the JFET (Q1) upon the voltage V across nodes 5 - 6 in Figure 3.11. This voltage (which is internal to Q1) is not experimentally measurable, but it must be accurately predicted if the calculated nonlinear response is to be accurate. We conclude that it is more important to accurately model the input coupling to Q1 than the coupling to a 50-ohm output load. We also note that the load will not be 50 ohms when we are interested in measuring and/or calculating the nonlinear response. These matters will be addressed in the next section.

REFERENCE

[3.1] J. J. Whalen and C. Paludi, "Computer-aided Analysis of Electronic Circuits - the Need to Include Parasitic Elements," International Journal of Electronics, Vol. 43, No. 5, 1977, pp. 501 - 511.

SECTION 4

MODELING THE NONLINEAR RESPONSE TO AMPLITUDE-MODULATED EXCITATION

4.1 Small-Signal Nonlinear Response to Amplitude-Modulated Signals

We are primarily interested in the nonlinear response of the JFET amplifier to amplitude-modulated excitation as outlined in the objectives of the effort discussed in Section 2.1. The leading term in a small-signal nonlinear analysis of amplitude-modulated input response is the square-law or second-order nonlinear term. Of special interest is the response at the amplifier tuned frequency (1.2 kHz).

4.1.1 Approximate Analysis - Power Series Model

A simple square-law nonlinear system without memory provides an approximate response to amplitude modulation. Figure 4.1 summarizes the essentials of such an analysis. Note that there are two low-frequency spectral responses directly related to the modulation frequency f_m. The fundamental component at f_m has amplitude $m|K|^2 H_2$ while the second harmonic at $2f_m$ has amplitude $|mK|^2 H_2/4$. If the modulation index $m = 0.5$, the second harmonic is 18 dB weaker than the fundamental. We shall concentrate our analysis and experimental measurements upon the response at f_m since it is larger, but we do recognize that the tuned amplifier would respond with an in-band response at the tuned frequency 1200 Hz to amplitude modulation at 600 Hz.

4.1.2 Second-Order Nonlinear Transfer Function Analysis

The power-series model does not suggest how one should introduce the frequency dependence of RF coupling to the nonlinearity in the amplifier or how to explicitly include the low-frequency audio gain of the amplifier. These difficulties are removed by modeling the system by the second-order term in a Volterra series and to express the second-order response in terms of nonlinear transfer functions. When this approach is carried out for the amplitude-modulated input, we find the

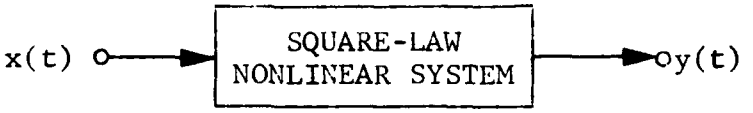

MODEL:

$$y(t) = a_2 x^2(t)$$

WHERE

$a_2 = H_2$, THE NONFREQUENCY-DEPENDENT POWER-SERIES COEFFICIENT

INPUT (AM-MODULATED CARRIER):

$$x(t) = K(1 + m \cos 2\pi f_m t) \cos 2\pi f_0 t$$

WHERE

K = PEAK AMPLITUDE OF CARRIER
m = MODULATION INDEX
f_m = MODULATION FREQUENCY
f_0 = CARRIER FREQUENCY

OUTPUT:

AT f_m –

$$y(t)\Big|_{f_m} = m|K|^2 H_2 \cos 2\pi f_m t$$

AT $2f_m$ –

$$y(t)\Big|_{2f_m} = \frac{m^2|K|^2}{4} H_2 \cos 4\pi f_m t$$

Figure 4.1 Power-Series Model - AM Excitation

output y(t) component at f_m to be given by

$$y_2(t)\Big|_{f=f_m} = \frac{m|K|^2}{4}\left[H_2(f_0+f_m,-f_0) + H_2(f_0,-f_0+f_m)\right]e^{j2\pi f_m t}$$

$$+ \text{complex conjugate} \qquad (4.1)$$

The first term in the bracket represents the contribution from the upper sideband (USB) caused by interaction of the input USB with the carrier in the nonlinearity. The second term represents the contribution from the lower sideband (LSB) caused by interaction of the input LSB with the carrier in the nonlinearity.

The output at the second harmonic of f_m is given by

$$y_2(t)\Big|_{f=2f_m} = \frac{m^2|K|^2}{8} H_2(f_0+f_m,-f_0-f_m)e^{j4\pi f_m t}$$

$$+ \text{complex conjugate} \qquad (4.2)$$

This term is contributed by the interaction of the USB and LSB in the nonlinearity. Calculation of the second-order nonlinear transfer function requires a circuit model for the amplifier including second-order nonlinearities.

4.1.3 Modeling the Nonlinear Amplifier

The dominant nonlinearity in the amplifier is the nonlinear dependence of drain current upon gate-to-source voltage v in Q1, the JFET transistor. Therefore, to second-order, the drain current is given by

$$i(v) = g_1 v + g_2 v^2 \qquad (4.3)$$

where $g_1 = g_m$ and g_2 is the second-order coefficient in a power-series expansion of the drain current in terms of the instantaneous gate-to-source voltage v. Figure 4.2 illustrates the

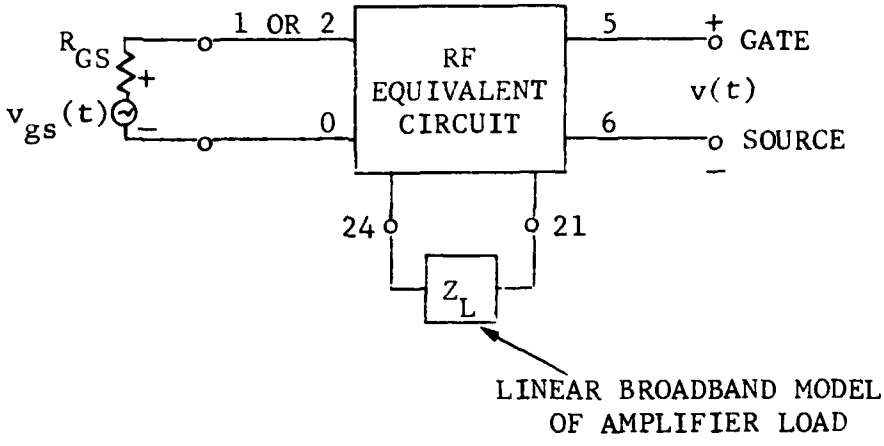

(a) First-order (Linear) Model

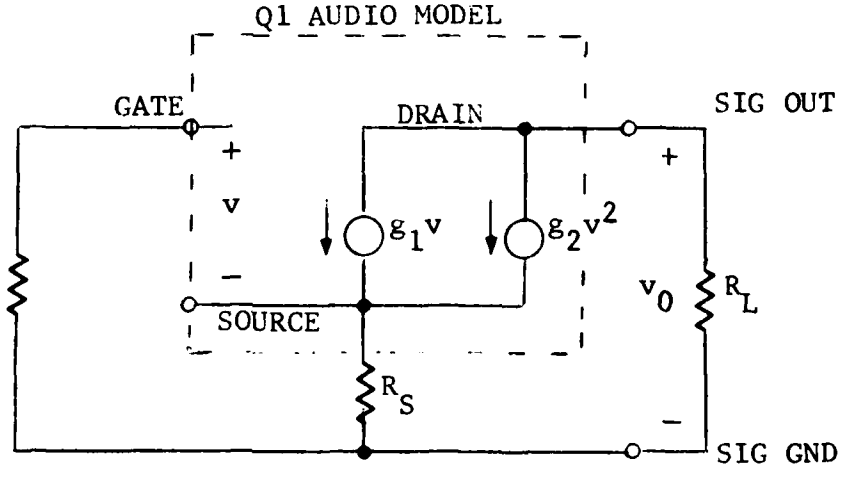

(b) Second-Order Equivalent Circuit of Amplifier at Audio Tuned Frequency

Figure 4.2 Modeling the Nonlinear JFET Amplifier

model. The input excitation source [Figure 4.2(a)] excites the RF equivalent circuit model to produce a linear response v(t) at the gate-to-source node pair. This transmission can be calculated by a linear analysis of the circuit model for the JFET amplifier developed in Section 3 and illustrated in Figure 3.11. The input excitation is connected to either nodes 1 or 2 depending upon whether normal signal input (node 1) or case-ground (node 2) excitation is desired. The response needed is the linear output at node pair 5 - 6 across branch B10 in Figure 3.11. Note that this calculation must be made with a broadband RF model of the "audio" load Z_L in place at node pair 21 - 24.

The next step is a second-order circuit consisting of a linear circuit excited by the dependent current source given by Eq. (4.3). Only the spectral components of g_2v^2 at f_m for amplitude-modulation excitation are of interest. Therefore, a linear circuit model valid at $f=f_m$ is all that is required to determine the amplifier output. Figure 4.2(b) shows such a model where we have retained only the equivalent resistance R_S between source and ground and the equivalent tuned-load resistance R_L between drain and ground. If we were interested in the second-order response to values of f_m other than at the amplifier-tuned frequency, it would then be necessary to use the more complete low-frequency circuit model such as that illustrated in Figure 3.4.

4.1.4 Calculation of the Second-Order Nonlinear Transfer Function

We have noted in Section 4.1.2 that the required second-order nonlinear transfer function H_2 depends upon the interaction at the nonlinearity of the USB, LSB, and carrier of the input amplitude-modulated signal. Figure 4.2(a) would be used to determine the magnitude and phase of each of these three separate spectral components at the gate-source node pair. It is quite appropriate here to observe that frequency-selective distortion that would, in general, be possible can be safely ignored since the modulated bandwidth ($2f_m$) of the input is very much less than the frequency selectivity of the RF equivalent circuit throughout the entire spectral regions of interest. With this approximation, the contribution to $y_2(t)$ at $f=f_m$ [see Eq. (4.1)] will be equal for both the sidebands. We may then express the output component in the form

$$g_2(t)\Big|_{f=f_m} = v_0(t)\Big|_{f=f_m}$$

$$= m|K|^2|H_2| \cos(2\pi f_m t + \varphi_2) \tag{4.4}$$

where

$$|H_2| = |H_2(f_0+f_m, -f_0)|$$

$$\varphi_2 = \underline{/H_2(f_0+f_m, -f_0)}$$

We may also at this point perform a direct calculation of the response of the model in Figure 4.2. Let

$$H_1(f) \triangleq \frac{V(f)}{V_{GS}(f)} \tag{4.5}$$

be the linear transfer function from input voltage source to the node pair 5 - 6. Then, at the node pair, we have

$$v(t)\Big|_{AM} \cong K|H_1| \ (1 + m \cos 2\pi f_m t) \cos(2\pi f_0 t + \varphi_1) \tag{4.6}$$

where

$$|H_1| = |H_1(f=f_0)|$$

$$\varphi_1 = \underline{/H_1(f=f_0)}$$

for an amplitude-modulated excitation given by

$$v_{gs}(t) = K(1 + m \cos 2\pi f_m t) \cos 2\pi f_0 t \tag{4.7}$$

The spectral component of dependent current exciting the network in Figure 4.2(b) at $f=f_m$ from Eq. (4.6) is

$$g_2\, m|KH_1|^2 \cos(2\pi f_m t + \varphi_1)$$

It follows by simple analysis of the Figure 4.2(b) circuit that

$$v_0(t) = -m g_2 \frac{R_L}{1 + g_1 R_s} |KH_1|^2 \cos(2\pi f_m t + \varphi_1) \quad (4.8)$$

is the desired nonlinear response to amplitude modulation. We also observe, by comparison with Eq. (4.4), that

$$|H_2| = g_2 \left(\frac{R_L}{1 + g_1 R_s} \right) |H_1|^2 \quad (4.9)$$

This factored form of $|H_2|$ will serve as a basis for estimating g_2 from experimental measurements of v_0. Note that dependence of the nonlinear response upon RF carrier frequency is entirely dependent upon the linear response H_1.

4.2 Measuring the Demodulated AM and Modeling the Spectrum Analyzer

4.2.1 The Experimental Setup

Before presenting the results of the model prediction of nonlinear response and comparison of the measured response with the prediction, it is appropriate to review the circumstances existing when the measurements were made. We have previously described in Section 2 the test amplifier and experimental configuration found necessary to obtain repeatable and reliable measured data. Tests were made with the amplifier excited by an HP 8640B Signal Generator for inputs above 1 MHz and by an HP 606B HF Signal Generator for signals between 50 kHz and 1 MHz. Both of these instruments have 50-ohm source impedances, calibrated output power, and calibrated modulation. Tests were performed at 50% AM ($m = 0.5$) and at an available carrier power of -20 dBm. The modulation frequency was the amplifier tuned frequency near 1200 Hz.

4.2.2 The Spectrum Analyzer Load

At -20 dBm available power excitation levels the nonlinear response from the amplifier with normal signal input excitation at 10 MHz is of the order of several millivolts. In the vicinity of nulls, nonlinear responses are of the order of 0.1 mV. Therefore, it is necessary to have a sensitive frequency-selective voltmeter to measure the nonlinear response. It is also necessary to have a high output-load-impedance for the amplifier load so that the amplifier will be realistically terminated. These requirements were met in the experimental setup by using a HP 3580A Spectrum Analyzer. This instrument has a scan mode that can be tuned to the 1200-Hz response, has good narrowband resolution, and has a 1-megohm input impedance over its 5-Hz to 50-kHz input spectral region. It also has a calibrated RMS voltmeter with excellent sensitivity. The basic complications with any experimental instrumentation used to measure the 1200-Hz response is that the instrument presents an entirely different load impedance to the amplifier at radio frequencies. The nonlinear response, particularly that for case-ground excitation, is critically dependent upon the impedance above about 100 MHz. Figure 4.3 shows the input impedance at the input terminals of the HP 3580A for the 10- to 500-MHz region on a Smith chart. Below 10 MHz, the impedance is approximately 1 megohm shunted by 30 pF. Note that between 160 and 170 MHz the impedance has a series resonance with about 10 ohms resistive resonant impedance. Between 305 and 310 MHz, a parallel resonance occurs with a resonant impedance of about 600 ohms.

In addition to having a seriously frequency-dependent input impedance, the HP 3580A has to be connected to the amplifier output terminals with a reasonable length of test cable. About three feet of 50-ohm coax cable, having a delay of about 1.5 ns per foot, was used in the measurements. In the presence of this cable, it is necessary to transform the analyzer impedance back toward the generator to the amplifier output terminals. Because the insertion phase shift of such a cable involves a number of wavelengths and the analyzer itself does not lend itself to a simple lumped equivalent circuit, it was judged inappropriate to attempt a lumped circuit model for the HP 3580A and its connecting cable. Predictions were made using the RF equivalent circuit in Figure 3.11 after independently calculating the equivalent R and L or C load at each RF excitation frequency for which a prediction was required.

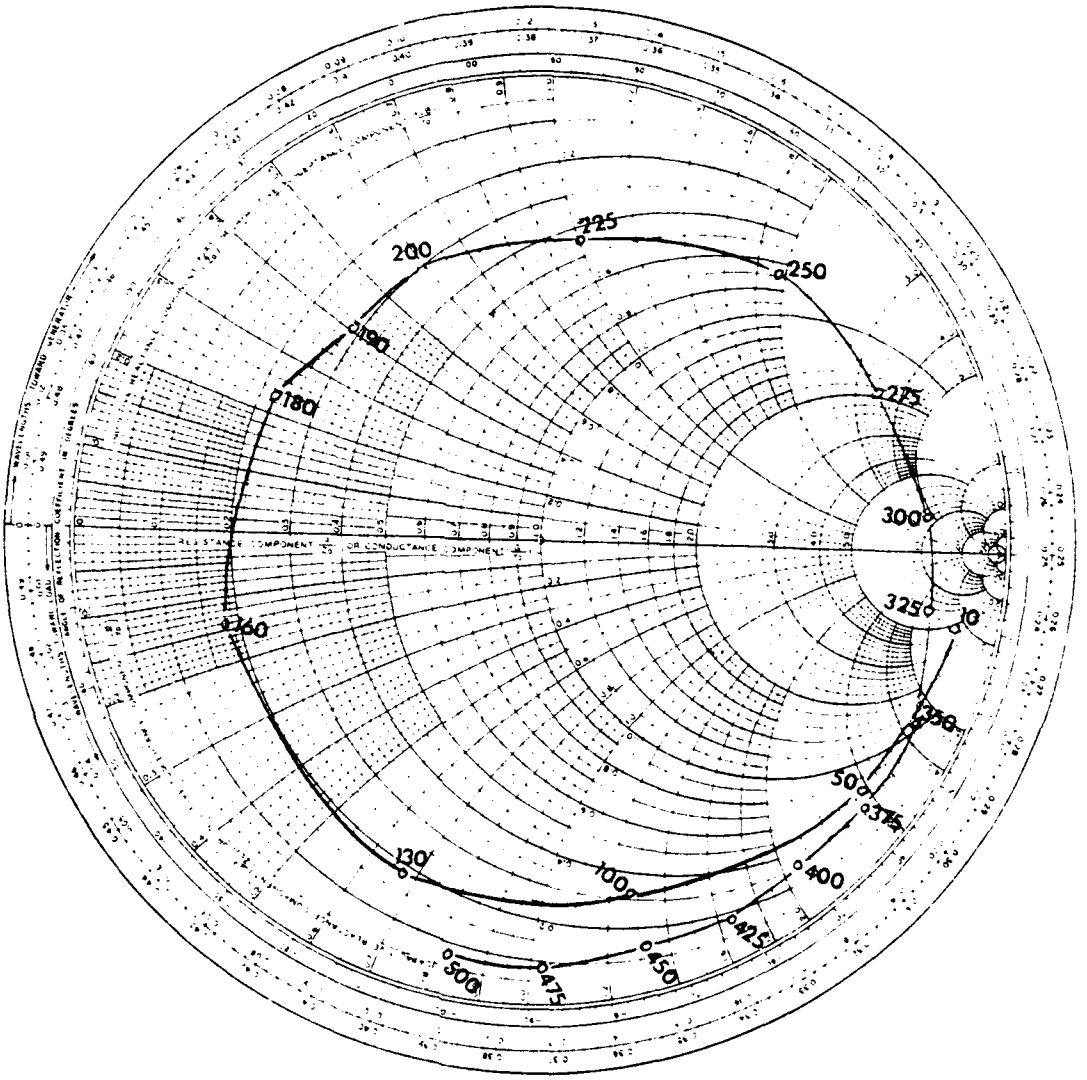

Figure 4.3 Input Impedance of HP 3580A Spectrum Analyzer for 10- to 500-MHz Band (R_0 = 50 ohms)

4.2.3 Reducing Experimental Measurements to Obtain $|H_2|$

Equation (4.4) provides the basis for obtaining an estimate of $|H_2|$ for experimental measurements of the 1200-Hz nonlinear response to amplitude modulation. We note first that $m|K|^2|H_2|$ is the peak voltage response at f_m for an amplitude-modulated input generator having a peak carrier amplitude of K volts, a source impedance of R ohms, and a peak sinusoidal modulation index m. Under these circumstances, the average carrier power P_c available from the signal generator is given by

$$P_c = \frac{1}{8}\frac{|K|^2}{R} = \frac{|K|^2}{400} \text{ watts} \tag{4.10}$$

The spectrum analyzer is calibrated in terms of RMS volts. If we let v_{0rms} be the RMS voltage obtained from the analyzer, we then obtain the relationship

$$\sqrt{2}\, v_{0rms} = m|K|^2|H_2| \tag{4.11}$$

Introducing Eq. (4.10) into (4.11) and solving for $|H_2|$, we obtain a relationship for an experimental estimate of $|H_2|$ given by

$$|H_2| = \frac{1}{\sqrt{2}}\frac{v_{0rms}}{4m\,R\,P_c} \tag{4.12}$$

Specializing this for $m = 0.5$, $R = 50$ ohms, and $P_c = 10^{-5}$ (-20 dBm), we obtain

$$|H_2| = \frac{1}{\sqrt{2}}\, v_{0rms}\Big|_{mV} \tag{4.13}$$

where v_{0rms} is in millivolts. It follows that

$$H_2\Big|_{dB} = -3 + 20\log_{10}\, v_{0rms}\Big|_{mV} \tag{4.14}$$

The decibel form given by Eq. (4.14) will be the basis of presenting the experimentally-measured data for comparison with the model prediction given by Eq. (4.9) which may also be obviously put in a decibel form.

A comment is in order regarding the choice of -20 dBm as the excitation level for the amplitude-modulation input carrier power. Measurements at 1200 Hz on the experimental amplifier indicate that the transition region from small-signal square-law nonlinear operation to a region where large-signal methods of analysis would be necessary occurs at an output level of about 3 volts RMS. The largest value measured for $|H_2|$ is about 44 dB. This occurs for normal signal input excitation at carrier frequencies below about 1 MHz. Using Eq. (4.14), this indicates that the output nonlinear response for -20 dBm input would be 224 millivolts RMS. If the input were raised to -10 dBm, a 20-dB increase in the output would occur, or an output level of 2.24 volts RMS would be expected. This is judged to be too close to the 3 volts RMS maximum. Hence, our choice of -20 dBm is a conservative choice. The input could be increased substantially at higher frequencies without approaching the large signal boundary. For example, in spectral regions above 100 MHz, where the nonlinear response is roughly 40 dB weaker, an increase in excitation level by 20 dB to 0 dBm would be permissible.

4.3 Comparison of Predicted and Measured Second-Order Nonlinear Transfer Functions

4.3.1 Normal Signal Input Excitation

Figure 4.4 shows the second-order transfer function obtained from the model and a comparison with measured data for excitation at the normal signal input (node pair 1 - 0). The spectrum analyzer load is in place at the output. The data and model estimate are in excellent agreement from 50 kHz to over 50 MHz with quite good agreement between 50 and 500 MHz. The experimental measurements were converted to $20 \log_{10}|H_2|$ using Eq. (4.14) as described in the preceding section. The model estimate is from Eq. (4.9) expressed in the form

$$20 \log_{10}|H_2| = 40 \log_{10}|H_1| + 20 \log_{10}\left(\frac{g_2 R_L}{1 + g_1 R_S}\right) \tag{4.15}$$

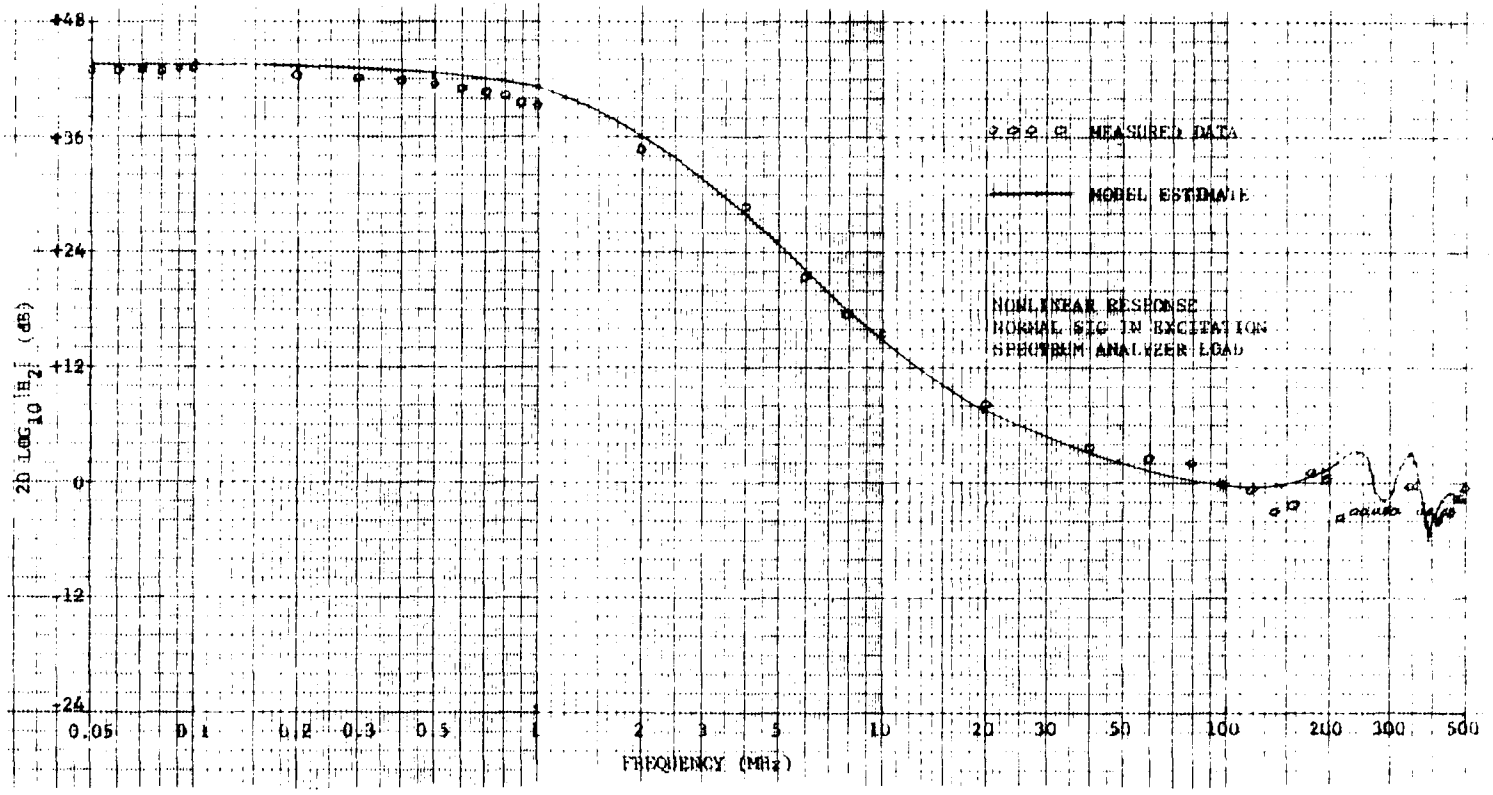

Figure 4.4 Second-Order Nonlinear Transfer Function for Normal Signal Input Excitation

$|H_1|$ is obtained by computer-aided analysis of the radio-frequency model given in Figure 3.11. For example, at 0.1 MHz, $|H_1| = 0.798$ or $40 \log_{10}|H_1| = -3.9$ dB. We have as yet not discussed a means for determining the numerical value of g_2 in Eq. (4.15). Values for $g_1 = g_m = 427 \times 10^{-6}$, $R_L = Q_L \omega L // 150K // 1000K = 126K$, and $R_S = 474 // 32.2K = 465$ ohms are all obtainable from the low-frequency model given in Figure 3.4 with values from Table 3-1. The numerical value of g_2 is determined by the nonlinear dependence of Q1 drain current upon gate-to-source voltage v. It is a constant that must be obtained by a measurement of the nonlinear distortion at one frequency or by determining the nonlinear parameter values of a JFET transistor model from a more complete drain current characteristic. Since either method involves measurements and we have distortion measurements, we can employ them directly without further modeling of the JFET nonlinearity. At 0.1 MHz we note from Figure 4.4 that $20 \log_{10}|H_2| = 43.5$ dB. Therefore, we have

$$20 \log_{10} \frac{g_2 R_L}{1 + g_1 R_S} = 43.5 + 3.9 = 47.4 \text{ dB}$$

This value is used at all frequencies across the 50-kHz to 500-MHz band. Since R_S, R_L, and g_1 are known, we can now also determine g_2 which we readily find to be given by

$$g_2 = \frac{234.4(1 + g_1 R_S)}{R_L} = 2.23 \times 10^{-3} \qquad (4.16)$$

This value for g_2 is to be compared with the value 2.19×10^{-3} obtained by Whalen, Paludi and Fang [4.1] in their effort to model Q1 in a similar amplifier.

4.3.2 Case-Ground Input Excitation

Figure 4.5 shows the second-order transfer function obtained from the model and a comparison with measured data for excitation at the case-ground input (node pair 2 - 0). The spectrum analyzer load is in place at the output. The model prediction and measured data agree well over the entire 50-kHz to 500-MHz band considering the complexity of the response above 30 MHz. Below 30 MHz, the second-order transfer function for case excitation is substantially less than that for normal signal input excitation. Above 30 MHz, the second-order

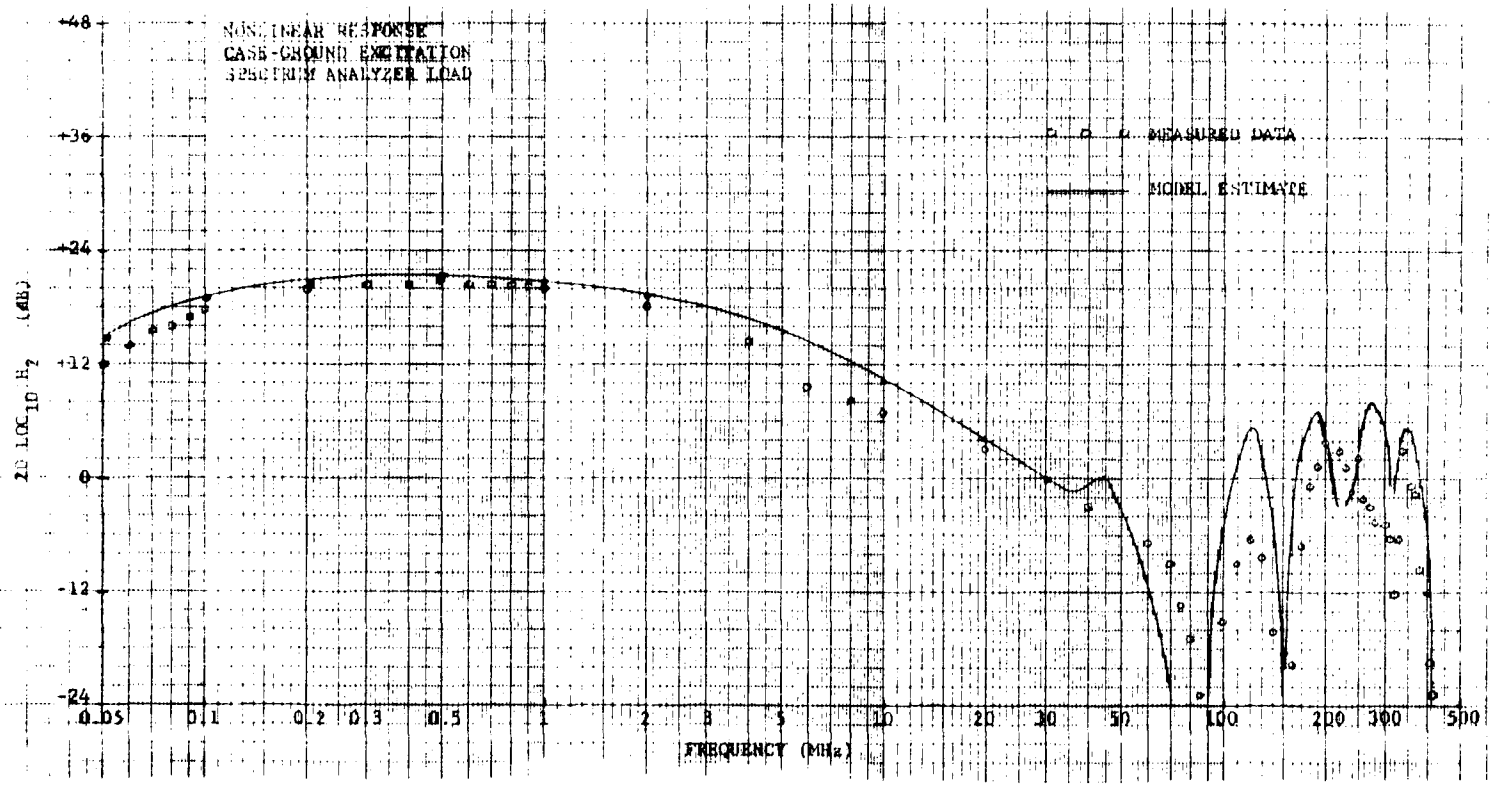

Figure 4.5 Second-Order Nonlinear Transfer Function for Case-Ground Input Excitation

transfer function is characterized by a series of deep peaks and nulls with a deep broad null near 85 MHz. The peaks above 100 MHz are of the same order strength as the rather "flat" not-so-deep peak and valley region for the normal signal input excitation. It is possible to identify in detail the cause of the behavior of both the normal and case-ground input frequency dependence. We shall discuss this subsequently. Note at this point, however, that in the 200 - 400 MHz region, several of the peaks for case excitation exceed the distortion that would be produced by excitation of the normal signal input port.

4.4 Discussion of the Nonlinear Model

4.4.1 Normal Signal Input Nonlinear Model Frequency Dependence

As we have observed on frequent occasions, the frequency dependence of H_2 is dependent upon the linear response of the linear high-frequency model through the term involving $H_1(f)$ in Eq. (4.15). $H_1(f)$ is the voltage gain [see Eq. (4.5)] from the input source to the gate-to-source node pair 5 - 6. For practical purposes, up to at least 100 MHz the input circuit that is effective in determining H_1 can be modeled by the simple circuit shown in Figure 4.6(a) and its equivalent in Figure 4.6(b) where we have identified the circuit components with the components in the amplifier. H_1 then follows and is given by

$$H_1 \cong \frac{V}{V_{IN}} = \frac{1}{1 + g_m R_S} \frac{1 + j\omega C_1 R}{1 + j\omega(C_1 + C_e)R} \tag{4.17}$$

The rest of the model largely has no impact upon the gate-to-source voltage except for minor effects impacting the input impedance to Q1 caused by the complicated load on the output.

4.4.2 Case-Ground Input Nonlinear Model Frequency Dependence

Physical explanation of the frequency dependence of H_1 for case-ground excitation is more complicated and can only be approximately dealt with in a simple manner. Figure 4.7(a) shows a simplified circuit model for the input coupling to Q1. Below roughly 10 MHz, the loading of Y may be ignored. Coupling from the source is principally through branches B40 (0.45 pF)

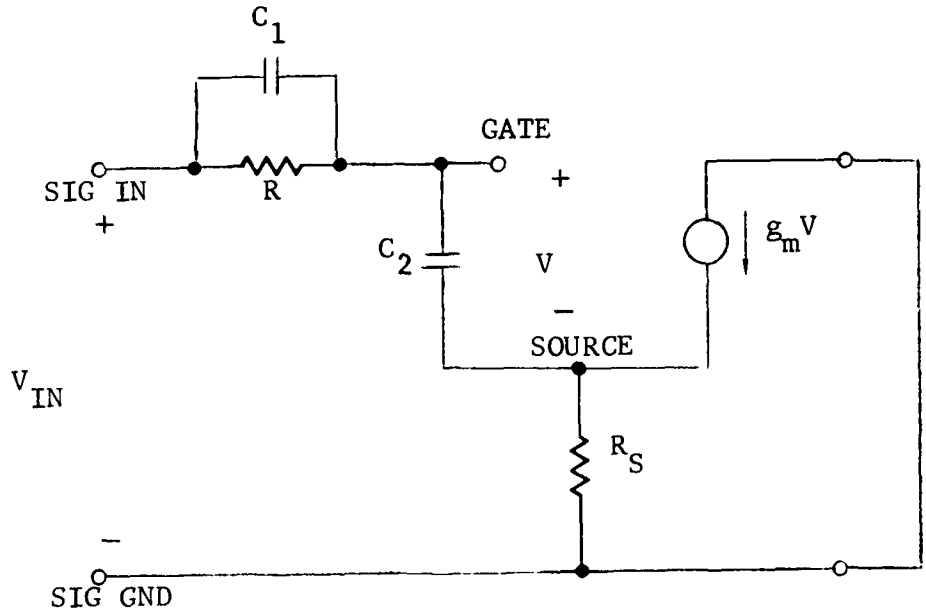

(a) Effective Input Circuit to Q1

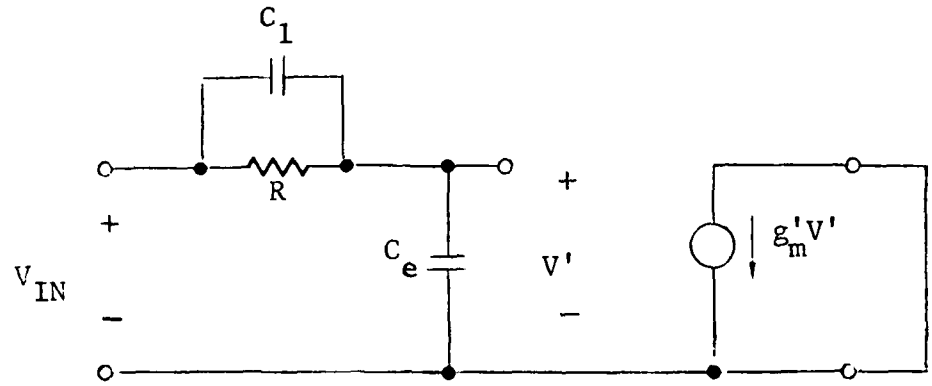

(b) Equivalent Input Circuit

$C_1 = CR3$

$C_2 = C_{11} + C_{GS}$

$R = R3$

$$g_m' = \frac{g_m}{1 + g_m R_S}$$

$$C_e = \frac{C_2}{1 + g_m R_S}$$

Figure 4.6 Input Circuits to Q1 for Normal Signal Input

and B41 (0.15 pF). The gate-to-source voltage of Q1 is exceedingly sensitive to currents through the PC etch capacitances in branches B40 and B41. Above roughly 10 MHz, the coupling network approaches a simple capacitor voltage divider with fixed insertion loss.

The complex frequency dependence of H_1 above 10 MHz is largely accounted for by shunt loading on the case-ground input source represented by Y in Figure 4.7(a). An appreciation of the impact of Y on H_1 can be obtained by examination of Figure 4.7(b) where we illustrate an approximate equivalent circuit representing the high-frequency loading of the amplifier output circuits on the case-ground input. Capacitance C is the aggregate of the PC etch capacitance in branches B42 and B43 plus the capacitance between the case of inductor L1 and nodes 9 and 16. From the point-of-view of node 2, nodes 9 and 16 are shorted by the low impedance of C3. (See Figure 3.11.) Inductance LA is the inductance LC5, LB is the inductance in the PC etch between nodes 0 and 29, LC is the inductance between nodes 24 and 29, and LD is the inductance between nodes 0 and 24. The spectrum analyzer load effectively is across the output. Near 85 MHz, capacitance C and the effective inductances between nodes (9,16) and 0 have a series resonance. This effectively shunts the case-ground node to signal-ground and blocks excitation of the JFET nonlinearity. This mechanism was confirmed by observing that the null in $|H_2|$ data was present in the model when the output at node pair (9,16) - 24 is either opened or shorted. (Note that this test cannot be done physically since shorting or removing the spectrum analyzer physically removes the ability to measure H_2.) It is interesting to note in passing that each of the elements involved in this resonance is a parasitic element. Establishing parameter values for these parasitic elements required much effort involving the model for the inductor L1 and, particularly, its asymmetry. The presence of the spectrum analyzer at the output produces the peaks and nulls in the data at frequencies other than near 85 MHz (see Section 4.2.2).

Finally, we observe that the presence of Y shunting the case-ground does not increase the nonlinear response to values greater than there would have been if it were absent, but instead simply loads the source down to reduce excitation of the Q1 nonlinearity.

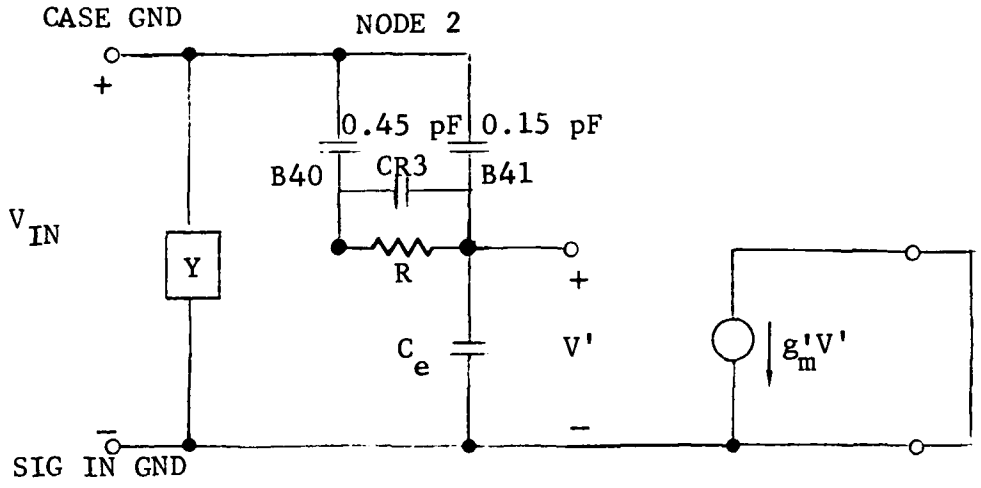

(a) Equivalent Input Circuit

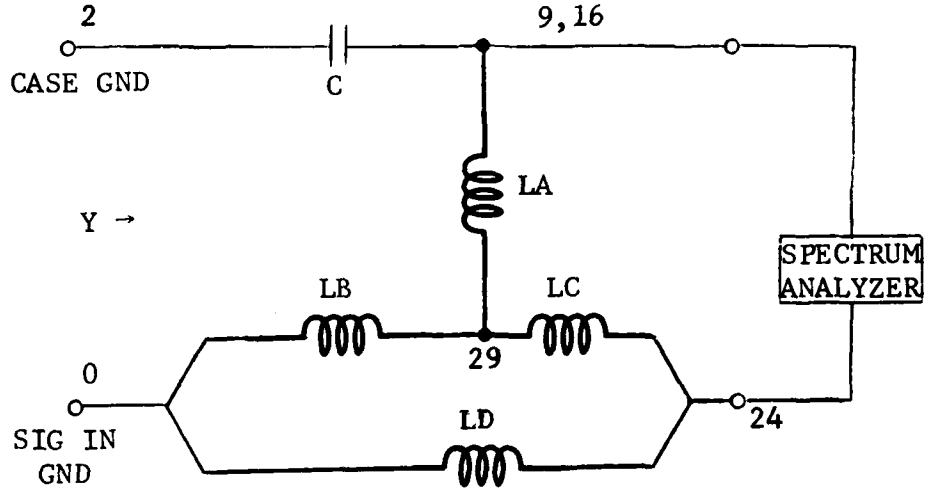

(b) Approximate Equivalent Circuit of Shunt Loading Admittance Y

Figure 4.7 Input Circuits to Q1 for Case-Ground Excitation

4.5 Using the Model to Predict an Equivalent Input to the Amplifier Caused by Nonlinear Distortion

It is interesting to utilize the modeling results to estimate the equivalent distortion referred to the amplifier input. Suppose that the case ground is excited at 200 MHz with a -30 dBm (10^{-6}) signal having 100% amplitude modulation. Assume that the source impedance is 50 ohms.

From Eq. (4.12), we have at the amplifier output

$$v_{0rms} = 4\sqrt{2}\ m\,R\,P_c\,|H_2|$$

From Figure 4.5 we note that $20\ \log_{10}|H_2|$ is is about +2 dB (x 1.26) for the experimental amplifier. With these parameters,

$$v_{0rms} = 4\sqrt{2} \times 1 \times 50 \times 10^{-6} \times 1.26$$

$$= 0.356 \text{ millivolts}$$

Now, the gain of the amplifier at 1.2 kHz is 26.6 dB (x 21.4). Hence, the nonlinear distortion referred to the amplifier input is 356/21.4 = 16.6 microvolts.

4.6 Comments on Amplifier Design Modification that Will Reduce the Nonlinear Distortion

The reason that the amplifier has significant nonlinear response to radio frequency excitation at the normal signal input terminals is simply that the design does not adequately attenuate such inputs before they reach the input to Q1. For example, inspection of Figure 4.4 shows that there is no attenuation of radio frequencies below 1 MHz and that the attenuation is only down about 20 dB above 100 MHz. The amplifier needs a good lowpass filter in its input.

To reduce the excitation of the nonlinearity for case-ground excitation, it is necessary to obstruct the coupling of signals to Q1 through the PC etch capacitance at nodes 1, 3, 4, and 5 through branches B39 - B41. An obvious means of

accomplishing this is to design a double-layer PC board with a conducting shield or gua·d between amplifier input nodes 1, 3, 4, and 5 and the case. This guard should be grounded to SIG GND at the input. Capacitance coupling from the excited case is then diverted to SIG GND rather than to the critical input nodes of the amplifier.

REFERENCE

[4.1] J. J. Whalen, C. A. Paludi, and T. F. Fung, "Applications of the Nonlinear Circuit Analysis Program NCAP," 1977 IEEE International Symposium on Electromagnetic Compatibility.


DA
FILM